Mafic alkaline metasomatism in the lithosphere underneath East Serbia: evidence from the study of xenoliths and the host alkali basalts

Journal Article

Mafic Alkaline Metasomatism in the Lithosphere underneath East Serbia: Evidence From Study of Xenoliths and the Host Alkali Basalts

V. CVETKOVIĆ, H. DOWNES, V. HÖCK, D. PRELEVIĆ, M. LAZAROV

Abstract

Effects of mafic alkaline metasomatism have been interpreted by study of East Serbian (SE Europe) mantle xenoliths and petrogenesis of their host alkaline rocks. Fertile xenoliths (addition of >10 %vol. of metasomatic clinopyroxene) and tiny assemblages found in depleted xenoliths are distinguished. The fertile lithology contains Ti-Al-Cr-rich clinopyroxene, Fe-rich olivine, Fe-Al-rich orthopyroxene and Al-rich spinel. The composition of this lithology is modeled by addition of 5-20 wt% of a basanitic-like melt to a refractory mantle. The small-scale assemblages occur as pocket-like, symplectitic or irregular deformation-assisted accumulations of metasomatic phases, generally composed of Ti-Al- and incompatible elements-rich Cr-diopside, Cr-Fe-Ti-rich spinel, altered glass, olivine, apatite, ilmenite, carbonate and feldspar, as well as relicts of a high-TiO_2 (~11 wt%) phlogopite. Textural relationships imply the following reaction: opx + Cr-rich sp ±phlogopite + Si-poor alkaline melt = Ti-Al-cpx + Ti-rich sp ± ol ± other minor phases. The inversion modeling, performed on least contaminated and most isotopically uniform host basanites, implies a source which is enriched in highly and moderately incompatible elements (~35-40xchondrite for U-Th-Nb-Ta, 2xchondrite for heavy rare earth elements) suggesting that the primary magma of the host basanites was not derived by melting of a homogeneous asthenospheric source. D_0 values of the calculated basanitic source are similar to D_0 values of anhydrous metasomatized mantle with small additions of metasomatic clinopyroxene and carbonate (~5 %) and with traces of ilmenite (~1 %) and apatite (~0.05 %). A schematic two-phase model involves percolation of CO_2-and H_2O-rich fluids, precipitation of metasomatic hydrous minerals and their subsequent breakdown due to the further uplift of hot asthenospheric mantle. This model uses a general idea of linking intraplate alkaline magmatism to lithospheric mantle sources enriched by sub-lithospheric melts at some time in the past.

Mantle metasomatism is generally believed to be responsible for small-scale heterogeneities within the lithosphere (Dawson 1984; Harte 1984, 1987; Menzies *et al*. 1987). Evidence from the study of mantle xenoliths entrained in alkali basalts proved to be particularly important for understanding the origin of such heterogeneities. Studies have shown that the major metasomatic agents are: (i) carbonatitic melts (Baker *et al.* 1998; Yaxley *et al.* 1998; Gorring & Kay 2000; Wang & Gasparik 2001), (ii) silicate melts (Menzies *et al.* 1987; Vannucci *et al.* 1998; Zangana *et al.* 1999; Gregoire *et al.* 2000; Kepezhinskas *et al.* 1995, 1996; Schiano *et al.* 2002) and (iii) fluids (O'Reilly & Griffin 1988; Baker *et al.* 1998; Gorring & Kay 2000; Larsen *et al.* 2003), the latter two having a wide range of compositions. All these agents produce different metasomatic styles recognized by changes in primary mantle mineralogy and specific enrichments in trace element composition.

It is widely accepted that mafic alkaline metasomatism is produced by infiltration of small amounts of alkaline melts genetically related to the host alkaline magmas (e.g. Dawson 2002). These metasomatic agents dissolve primary orthopyroxene (±spinel) and precipitate secondary clinopyroxene and spinel, along with other minor phases such as apatite, ilmenite or carbonate. The metasomatic phases are sometimes found filling veinlets and patchy accumulations within depleted xenoliths. In addition, the same xenolith suites commonly contain granular clinopyroxene-rich lherzolite or wehrlite xenoliths, interpreted as products of

similar melt-rock interactions (e.g. Carpenter *et al.* 2002).
A detailed understanding of the effects of mafic alkaline metasomatism is usually difficult to achieve because of the following problems: (i) primary metasomatic products and textural relationships may often be destroyed or/and superimposed with those resulting from interaction with the host magma during magma ascent or immediately before eruption (e.g. Klügel 1998), and (ii) compositional changes caused by carbonatitic melts/fluids usually occur roughly concomitantly with silicate metasomatism, producing an overlap in geochemical effects (Neumann *et al.* 2002; Rivalenti *et al.* 2004). In this context, the information provided by a careful study of textural relationships and mineral compositional variations within the presumed metasomatic associations is essential. Recognition of secondary associations which texturally and compositionally appear to be unrelated to the host magma are very important for proving that these metasomatic associations genuinely originate in the mantle. Additionally, significant information about alkali silicate metasomatism can be potentially provided from the study of the host rocks. It is generally accepted that alkaline rocks which host mantle xenoliths, although having a strong asthenospheric signature, usually require a metasomatic component believed to reside in the lithosphere (e.g. Wilson & Downes 2006, and references therein). Because these rocks are fairly homogeneous isotopically, it is beleived that this metasomatism occurred shortly before the eruption and xenolith capture. It is, therefore, logical to suppose that these lithospheric domains, which are believed to have played role in petrogenesis of host alkaline rocks, may be compositionally (and texturally?) similar to metasomatic associations found in xenoliths. In this paper we revisit the problem of mafic alkaline metasomatic effects in mantle xenoliths from East Serbia. A larger xenolith sample collection has been studied for mineral major (EPMA) and trace element (laser ablation-inductively coupled plasma-mass spectrometer - LA-ICP-MS) compositions and the new data are discussed together with some previously published results (Cvetković *et al.* 2004 *b*). We present new textural and mineral chemistry evidence which provides better insight into these metasomatic events. In addition, we report a new set of whole rock ICP-MS trace element data on host basanites and perform the quantitative inversion modeling in order to infer the mineralogy of their magmatic source. These results were used to compare the inferred mantle source with the metasomatic associations observed in the studied xenoliths. Consequently, we offer a model in which mafic alkaline metasomatic associations, similar to those observed in the studied xenoliths, plays an important role in the petrogenesis of the host rocks.

Characteristics of the local upper mantle and host volcanism

The studied mantle xenoliths are found in Paleogene basanites of East Serbia (SE Europe). The characteristics of the main xenolith lithologies representing the East Serbian Lithospheric Mantle (ESLM) are reported by Cvetković *et al*. (2004 *b*) and summarized in Table 1. The predominant lithology is composed of very depleted harzburgite and clinopyroxene-poor lherzolites. Cvetković *et al.* (2007) discussed the problem of the very high degree of depletion and suggested that the mantle segment underneath East Serbia is similar to sub-arc oceanic mantle and may represent a slice of Tethyan oceanic lithosphere accreted during convergence. A sub-lithology of spinel-poor, orthopyroxene-rich olivine websterite xenoliths is interpreted to have originated by crystallization of high-Mg and silica120 saturated magmas (Cvetković *et al.* 2007). The existence of such magmas is an independent evidence for the existence of ultra-depleted mantle underneath the region. Various

subordinate xenolith lithologies containing secondary clinopyroxene were attributed to the effects of mafic alkaline metasomatism. Cvetković *et al.* (2004 *b*) described some textural relationships of these presumed metasomatic assemblages and reported trace element patterns of secondary clinopyroxene. Our study focuses on this lithology.

The East Serbian Paleogene alkaline rocks occur as relicts of small eroded monogenetic volcanoes along the western margin of the Carpatho-Balkanides (Jovanović *et al.* 2001; Cvetković *et al.* 2004 *a*). A detailed geochemical study of these rocks, including Sr, Nd, Pb and Hf isotopes, will be published elsewhere, and here we present only a selected set of our data. This alkaline magmatism originated within an orogenic setting as small pulses of magma between 60 Ma and 40 Ma ago (Jovanović *et al.* 2001; Cvetković *et al.* 2004 *a*). Ten localities of these rocks are known and at two of them, Sokobanja and Striževac, mantle xenoliths are present (Cvetković *et al.* 2004 *b*). The rocks are olivine- and clinopyroxene134 phyric and range in composition from basanites and olivine tephrites to tephriphonolites. Their isotope characteristics and trace element patterns are generally similar to alkaline rocks of the Central European Cenozoic Volcanism (e.g. Wedepohl & Baumann 1999), which are usually interpreted as derived by partial melting of mixed asthenospheric and lithospheric sources (Wilson & Downes 1991). However, mantle xenolith-bearing basanites from Sokobanja are characterized by uniformly low $^{87}Sr/^{86}Sr$ ratios (0.7029-0.7035) and can be potentially considered as derived from nearly pure asthenospheric melts. This assumption will be addressed in part where the mantle source characteristics of these lavas are discussed (see below).

Analytical methods

New major element microprobe data of minerals from these metasomatic associations are given in Table 2. The data were obtained using a wavelength-dispersive (WDS) electron microprobe at the University of Frankfurt. The analytical conditions are summarized by Cvetković *et al.* (2007). Additional mineral chemical data used here can be found in Cvetković *et al.* (2004 *b*) and Cvetković *et al.* (2007a, 2007b).

Trace element concentrations in minerals were determined at the University of Frankfurt using an *in situ* laser ablation inductively coupled plasma mass spectrometry (LA153 ICP-MS) technique using a New Wave Research LUV213TM ultraviolet Nd_Yag laser coupled with a Finnigan MAT ELEMENT2TM. The pulse frequency of 10 Hz, pulse energy in the range of 03-1.2 mJ and spot size between 30⌠m and 150⌠m were used. The USGS BIR 1-G glass (Eggins *et al.* 1997) and NIST612 glass (Pearce *et al.* 1997) were used as external standards. Silica was used as an internal standard. Trace element concentrations in olivines from a symplectite-bearing Mg-rich dunite xenolith (SB-M-3) and from a Fe-rich dunite xenolith (SB-M-1), as well as in olivines from refractory peridotite xenoliths (an average analysis from SB-M-4 and SB-M-5) are reported in Table 3a. Only three clinopyroxene crystals from metasomatic pockets were successfully ablated and their analyses are given in Table 3b, along with compositions of interstitial clinopyroxene and clinopyroxene in a lenticular symplectite from the Mg-rich dunite xenolith.

Trace element concentrations in whole rock samples of host Sokobanja basanites (Table 4), which were used for geochemical modeling, were done by an ICP-MS technique in ACME Analytical Laboratories Ltd. (Vancouver BC, Canada).

Results

Petrography and mineral chemistry of metasomatized xenoliths

Here we present characteristics of the mantle lithologies that appear to be related to enrichment by mafic silicate alkaline melts and describe newly observed textural relationships. For more general information on the xenolith petrography the reader is referred to Cvetković *et al.* (2004 *b*). The metasomatic lithologies are recognized as fertile xenoliths (addition of >10 vol% metasomatic clinopyroxene) and also as tiny metasomatic assemblages situated within depleted xenoliths (addition of <<5 vol% metasomatic clinopyroxene). Clinopyroxene (±olivine) megacrysts and Fe-rich dunite xenoliths are also present but they are not addressed here, except for comparison. Cvetković *et al.* (2004 *b*) demonstrated that these represent deep-seated magmatic cumulates.

The fertile xenoliths are represented by undeformed and protogranular clinopyroxene182 rich lherzolite and spinel-rich olivine websterite xenoliths. The lherzolites have the highest modal contents of green clinopyroxene (>20 vol%) in the ESLM xenolith suite. The clinopyroxenes show a spongy texture (Figure 1a), suggesting incipient melting. Similar textures are found in many xenolith suites and are especially frequent in wehrlite xenoliths (Yaxley *et al.* 1991; Xu *et al.* 1996; Weichert *et al.* 1997; Carpenter *et al.* 2002, etc.). The olivine websterite xenoliths are predominantly composed of tabular and undeformed orthopyroxene, smaller and less abundant olivine, and interstitial spongy greenish clinopyroxene. Spinel is particularly abundant (>2 vol%) and always appears as coarse190 grained accumulations associated with clinopyroxene (Figure 1b).

The clinopyroxene-rich lherzolite and spinel-rich websterite xenoliths are very similar in terms of mineral chemistry (Cvetković *et al.* 2004 *b*). They both contain high-Ti-Al-Cr clinopyroxene (~1 wt% TiO_2, 5-7 wt% Al_2O_3, 1-1.5 wt% Cr_2O_3), Fe-rich olivine (Mg# <88), Fe- and Al-rich orthopyroxene (Mg#~88, Al_2O_3 up to 6 wt%) and Al-rich spinel (Cr#=0.14-0.4).

In depleted peridotite xenoliths, secondary patchy and pocket-like mineral accumulations are also very common. They are composed of euhedral/subhedral clinopyroxene, xenomorphic spinel and altered glass, but substantial amounts of olivine, apatite, ilmenite, carbonate and feldspar are often present. Relicts of a high-TiO_2 (~11 wt%) phlogopite were found in one harzburgite xenolith (Cvetković *et al.* 2004 *b*). Textural evidence of orthopyroxene dissolution and formation of clinopyroxene selvages (Figure 1c), precipitation of new spinel (Figure 1d,e), and spinel dissolution and overgrowths is present (Figure 1e, analyses 12-14 in Table 2). The spinel owegrowths are remarkably similar to those found in xenoliths from northern Tanzania (Dawson 2002, Fig.3, p. 1755), which are interpreted as the result of Fe-Ti silicate melt metasomatism. In some pockets clinopyroxene occurs as fairly euhedral phenocryst-like crystals associated with tiny spinel and completely enclosed by carbonate (Figure 1f). Euhedral terminations of crystal faces suggest that clinopyroxene crystallized in an open space.

Generally, clinopyroxene in all these metasomatic assemblages is Ti-Al-rich Cr210 diopside (Table 2a, 1-9). Cr-spinels show variable composition but have generally higher Cr# and Fe and Ti contents (Table 2b, 1-7) in comparison to discrete primary spinel grains. Carbonate is Mg-bearing calcite with 1-3 wt% MgO. Apatite has low totals (<96.5 wt%), suggesting that substantial amounts of halogens may be present. Ilmenite has high MgO contents (~8 wt%). Feldspars vary from Ca-rich plagioclase to Na-rich K-feldspar, compositionally similar to feldspars found in other mantle xenoliths (e.g. Delpech *et al.* 2004).

Apart of such accumulations, dominated by freely crystallized euhedral clinopyroxene crystals, there is evidence of metasomatic reactions that were probably assisted by deformation. These assemblages were observed only in rare, slightly deformed xenoliths. Secondary minerals occupy the space between partially disrupted and re-arranged spinel grains and surrounding silicates. Figure 2a shows a sheared zone in a harzburgite xenolith containing spinel aggregates composed of scattered irregular grains, which sometimes display a jigsaw-puzzle texture (Figure 2b,e). Back-scattered electron (BSE) images show that the spinel has spongy rims that suggest melting and resorption (Figure 2c,d). An assemblage of clinopyroxene and olivine neoblasts, orthopyroxene relicts, and a non-stoichiometric mixture of phyllosilicates (Table 2d, analysis 5) is found adjacent to the spinel rims (Figure 2d). Similar spinel decomposition is found in metasomatized Yitong xenoliths (Xu *et al.* 1996; Fig. 3a, p. 409). Clinopyroxene in these associations is Al-Ti-rich and cannot be distinguished from that in the above-described patchy pockets. This is a very important observation implying that infiltration of a melt of similar composition, and not the host-melt-xenolith interaction is responsible for the origin of both secondary assemblages.

A particular textural type we believe belongs to the microscopic metasomatic assemblages (see discussion below) is seen in clinopyroxene-spinel-olivine symplectites. These were found only in two Mg-rich dunite xenoliths and occur in two textural forms. Lenticular or nest-like symplectites are around 1-2 mm in length and ~1 mm wide and texturally resemble the above-mentioned metasomatic patches (Figure 3a). They consist of fine-grained intergrowths of clinopyroxene, olivine and spinel in modal proportions of roughly 3:2:1. In a two-dimension profile (Figure 3a) clinopyroxene forms the basis of the symplectite aggregate, while olivine and spinel display a variety of shapes: rod-like, cylindrical, semi-circular, vermicular, etc. The other textural forms are intergrowths that do not show the well-confined outer forms seen in the lenticular symplectites. They rather appear as aggregates of tiny vermicular spinels in association with coarser olivine and clinopyroxene (Figure 3b). Olivine from symplectites and intergrowths has generally the same composition (~Fo_{90}) as adjacent olivine crystals unrelated to symplectitic forms. They are slightly less magnesian in comparison to olivine in depleted xenoliths. Spinel in the symplectite is slightly richer in FeO, TiO_2 and Al_2O_3 in comparison to discrete spinel grains from the same xenolith and differs from secondary spinels from pocket accumulations in having lower Cr#s (Table 2b, 8-11). Clinopyroxene from symplectite shows high Al_2O_3 (4.5-7 wt%), Na_2O (0.7-1.1 wt%), along with irregular but high TiO_2 (0.2-1.1 wt%) and Cr_2O_3 (0.9-3.6 wt%) contents (Table 2a, 10-14) and is generally similar in composition to clinopyroxene from metasomatic pockets (see below).

Metasomatized xenoliths - LA-ICP-MS data

Olivine from an Fe-rich dunite (Table 3a, sample SB-M-1) is richer in Li (>2 ppm), Ca (~1500 ppm), Sc (>5.5 ppm), Ti (~50 ppm), Mn (~1500 ppm) and Cr (~300 ppm) and poorer in Ni (~2600 ppm) than olivine from the symplectite-bearing Mg-rich dunite (SB-M-3) (Li<1.5 ppm, Ca ~1000 ppm, Sc >5.5 ppm, Ti<10 ppm, Mn ~1200 ppm, Cr ~150 ppm, Ni ~3500 ppm). Olivines from harzburgite xenoliths (SB-M-4 and SB-M-5) have the lowest contents of all measurable elements (e.g. Li<2 ppm, Ca~750 ppm, Sc<4.5 ppm, Ti<5 ppm, Mn~1000 ppm and Cr~ppm) coupled with the highest Ni contents (>3700 ppm). Given that all these elements except Ni behaves incompatibly in olivine in terrestrial olivine-melt systems (e.g. Karner *et al.* 2003), it can be concluded that the olivine from the symplectite264 bearing dunite is less enriched than olivine from the Fe-rich dunite but comparatively more

enriched than olivine from depleted xenoliths. This suggests that the olivine from symplectite266 bearing dunite most probably underwent cryptic metasomatic enrichment.
Multi-element patterns of the studied clinopyroxenes are illustrated in Figure 4. Euhedral clinopyroxene from pocket accumulations displays the highest contents of all trace elements and has the most LREE-enriched pattern ($[La/Lu]_N$~8). On the primitive mantle270 normalized diagram it shows a steady decrease of concentrations from the most incompatible towards the less incompatible elements. The exceptions are Rb and Ba that have an order of magnitude lower normalized concentrations than adjacent Th. Clinopyroxene from clinopyroxene-spinel-olivine symplectites displays a flat REE pattern ($[La/Yb]_N$~1) with a slight increase of concentrations from Gd to Lu. Mantle-normalized values of the highly incompatible elements are low with the exceptions of positive spikes at U, Pb and Sr. Discrete interstitial clinopyroxene from the same dunite sample has a roughly similar pattern as does the symplectitite clinopyroxene. However, the former has slightly lower concentrations of LREE and lacks positive anomalies at U and Pb. For comparison, trace element patterns of residual clinopyroxenes from harzburgite xenoliths are also shown. They exhibit a moderately LREE-enriched ($[La/Lu]_N$=3.5-10) pattern with low concentrations of HREE (e.g. Yb = 1.4-2.2xchondrite) and a pronounced peak at Sr.

Petrochemistry of the host volcanics

In the modeling only the Sokobanja mantle xenolith-bearing rocks were used. The rock samples of other locality where xenoliths were found (Striževac) are more heterogeneous, some having increased K_2O contents of up to 1.66 wt% and they were omitted. The chemical analyses of Sokobanja mantle xenolith-bearing mafic alkaline rocks are given in table 4. All samples are olivine (Fo_{76-86}) ±clinopyroxene (Mg# 75-85) phyric with groundmass consisted of clinopyroxene (Mg#>70), nepheline, plagioclase feldspar (An~60) and Ti-bearing magnetite (TiO_2~15 % wt.). They have high Mg# (~70) and high concentrations of incompatible elements (Ni mostly > 200 ppm and Cr > 450 ppm). On the whole-rock MgO vs Fe_2O_3 correlation diagram (Figure 5) they plot close to the equilibrium line of primitive mantle melts with no evidence of fractionation. Five samples show effects of small olivine accumulation (<6-7 %wt.) which could have negligible effects on trace element concentrations used in modeling (<<<1 % relative). The samples show low Sr (~0.7031) and high Nd (~0.5129) initial isotope ratios (Jovanović et al. 2001) and that indicates that they represent fairly uncontaminated magmas. Therefore, no correction of low pressure processes was necessary.

Discussion

Different styles of mantle modification

Characteristics of East Serbian xenoliths indicate that modifications of the lithospheric mantle generally occurred (i) by direct crystallization of alkaline magmas and (ii) by various melt-peridotite reactions. The latter process is the focus of this study. Direct crystallisation was responsible for formation of clinopyroxene/olivine megacrysts and high-Fe dunite xenoliths as suggested by Cvetković *et al.* (2004 *b*). They reported similarities between megacryst clinopyroxene from the ESLM and clinopyroxene megacrysts from alkaline basalts of the Pannonian Basin (Dobosi & Jenner 1999; Dobosi *et al.* 2003). Similar xenoliths/xenocrysts are commonly found in alkaline basalts worldwide (Aoki & Kushiro 1968; Irving 1974; Wilshire & Shervais 1975; Dal Negro *et al.* 1989; Righter & Carmichael 1993; Shaw & Eyzaguirre 2000; Brizi *et al.* 2003, among others) and in most cases

interpreted in terms of deep-seated cumulates. On the other hand, the formation of the enriched assemblages described above requires a mechanism other than direct magmatic crystallization. In the discussion that follows we present evidence that both fertile xenoliths and microscopic metasomatic assemblages originated due to various melt-wallrock reactions.

Origin of fertile xenoliths: high melt/peridotite ratio reactions

Cpx-rich lherzolite and olivine websterite xenoliths show similar textures as depleted xenoliths but their modal composition and mineral chemistry are much too fertile to represent fragments of residual mantle. Their clinopyroxene exhibits generally similar trace element patterns as the clinopyroxene megacrysts (Cvetković *et al.* 2004 *b*), suggesting that they are also related to alkaline magmas. However, it is unlikely that these pyroxene-rich lithologies formed by direct magmatic crystallization as suggested above for the megacrysts, because they contain orthopyroxene, a phase that is not on the liquidus in Si-undersaturated magmas (Ghiorso & Carmichael 1987). The possibility that they represent mixtures of residual mantle peridotites and crystal cumulates from mafic alkaline magmas is also unlikely. Their orthopyroxene is too rich in Al and Ca to be accounted for by simple addition of Fe-rich olivine and clinopyroxene to a harzburgite. By contrast, the compositional trends can be explained by melt-rock interactions. Figure 6 illustrates compositional changes of the depleted mantle due to addition of a basanitic melt. We recalculated bulk composition of the xenoliths using their modal analyses and chemistry of present minerals. The residual mantle is represented by average harzburgite and lherzolite of this xenolith suite. The average major element analysis of the host basanites was used as a proxy for the composition of mafic alkaline metasomatic melts. Accordingly, the calculated bulk Al_2O_3, CaO and TiO_2 contents of the fertile xenoliths can be obtained by addition of 5-20 wt% of a basanitic melt to a refractory mantle. Figure 6 also shows that addition of pure cumulitic material (80 % clinopyroxene and 20 % olivine) cannot produce a decrease in bulk CaO/Al_2O_3 ratio of the residual mantle lithology.

This suggests that the fertile xenolith lithology could have originated by refertilization of residual mantle regions by relatively Fe-rich alkaline basaltic melts. Similar compositional and textural changes in mantle peridotites are generally believed to be confined to the wall347 rocks along magmatic conduits, i.e. in the area of high melt/wall-rock ratio (Kempton 1987). Xu *et al.* (1996) report a linear change in composition from lherzolite to orthopyroxene349 bearing wehrlite and finally to orthopyroxene-free wehrlite and interpret this as resulting from advancing melt-peridotite reactions. Such a scenario proposes an infiltration of melts and their subsequent equilibration with the surrounding peridotite. Moreover, it also suggests that, along with precipitation of new secondary Ti-Al clinopyroxene, the already existing mantle minerals underwent detectable changes in composition, e.g. a decrease of Mg# in olivine and orthopyroxene and an increase of Al_2O_3 and CaO in orthopyroxene and Al_2O_3 in spinel. Such metasomatic changes require time and provide evidence that the reactions occurred *in situ* in the mantle rather than due to direct contact with the host magma. The occurrence of spongy clinopyroxene also argues against the second possibility. It is obvious that the spongy textures formed by a later thermal event, probably during entrapment of the xenoliths.

Frozen textures: patchy-pocket-like, deformation-assisted and symplectitic assemblages

Many authors (e.g. Yaxley *et al.* 1998; Coltorti et al., 1999, among others) argued that the pocket-like and vein assemblages found in mantle xenoliths originated *in situ* in the lithosphere. Following their arguments it can be emphasized that the secondary assemblages found in ESLM xenoliths are different from the phase associations found in host-related veins

because: (i) the latter often cut the whole xenolith, (ii) they contain Fe-rich and Cr-poor pinkish clinopyroxene, pure Ti-oxides and nepheline, and (iii) they usually produce Fe-rich rims on surrounding olivines. In contrast, the presumed *in situ* metasomatic aggregates contain greenish Cr-rich clinopyroxene and usually do not produce any effect on surrounding olivine. Figure 7 shows TiO_2 wt% vs Fe^{3+} variations for spinel and Fe-Ti-oxides in various associations of ESLM xenoliths. Ferric iron was calculated by accepting that spinel represents solid solution between $R^{2+}R^{3+}O_4$ and $R^{2+}R^{4+}O_4$. Most spinels in metasomatic pockets display an increase in TiO_2 that is not accompanied by substantial increase of Fe^{3+} concentrations, as seen for spinels that reacted with the host. Only a few pocket spinels show higher Fe^{3+} contents that can be related to shallow-level interaction between the host magma and spinel, which was not recognized texturally.

In general, these metasomatic assemblages are texturally similar to xenolith-hosted secondary mineral associations usually attributed to mantle metasomatism (e.g. Ionov *et al.* 1994; Zinngrebbe & Foley 1995; Wullf-Pedersen *et al.* 1996, 1999; Ionov *et al.* 1999). It is, however, highly possible that the observed textural relationships do not represent the original textures inherited from the mantle. Some aggregates in pockets could have formed due to decompressional or/and fluid-induced melting of earlier metasomatic phases followed by rapid crystallization of the melt. That is indicated by the occurrence of euhedral clinopyroxene and quench-like spinel crystals in some pockets. Decomposition of pre-existing metasomatic minerals is also suggested by the presence of phlogopite relicts in one sample. Given that all present metasomatic minerals are anhydrous, it can be concluded that this decomposition was an open-system process in which fluids released from phlogopite could leave the system. This implies that a metasomatic phase had formed in the lithosphere before the xenoliths were captured by basanitic magma.

Textures of frozen reactions found in slightly deformed xenoliths further suggest that at least some metasomatic reactions occurred *in situ* in the ESLM. Puzzle-like disintegrated spinels with spongy/recrystallized Ti-rich rims found along sheared zones in such xenoliths indicate that infiltration of metasomatic melt was assisted by deformation. Evidence for similar magmatic processes related to localized deformation was reported from a xenolith from the Pannonian Basin (Falus *et al.* 2004). It is highly unlikely that such textural relationships could originate after the xenolith capture. Post-entrapment deformation within xenoliths is related to thermal stress and release of internal fluids upon decompression and commonly gives rise to brittle cracking exclusively (Nicolas 1986, Wilshire & Kirby 1989, Klügel 1998).

Clinopyroxene-spinel-olivine symplectites are texturally similar to symplectites in the Horoman peridotite (Morishita & Arai 2003). However, the symplectites in ESLM xenoliths lack orthopyroxene and cannot be attributed to garnet breakdown reactions (Smith 1977). Zingrebbe & Foley (1995) mention conspicuous, millimetre sized symplectic intergrowths of clinopyroxene and spinel surrounded by thick margins of phlogopite in Gees xenoliths and they speculated that they may have formed after previous amphibole. To characterize the symplectites occurring in ESLM xenoliths we use the composition of clinopyroxene because this mineral shows relatively large compositional variations and occurs in a variety of textural assemblages. Major element compositional variations of texturally different clinopyroxenes are illustrated in Figure 8. Regarding the symplectite-related clinopyroxene the following conclusions can be derived: (i) it is clearly compositionally different from clinopyroxene megacrysts and from those related to reactions with the host, (ii) it generally follows the

compositional trends of clinopyroxenes believed to be melt/peridotite reaction products, and (iii) it is more similar in composition to small pocket clinopyroxene than to coarser clinopyroxene from fertile lherzolite and websterite xenoliths. Both symplectite clinopyroxene and clinopyroxene from metasomatic pockets have high Al_2O_3, TiO_2 and Na_2O contents, coupled with high Mg# and very high Cr_2O_3 contents. Similarities in trace element patterns of clinopyroxene from symplectites and those from overgrowths around orthopyroxene (Cvetković *et al.* 2007b) indicate that dissolution of orthopyroxene may have been involved in their genesis.

The above characteristics suggest that metasomatic pockets and symplectites originated in a similar way involving interaction between mantle peridotite and infiltrating melts. In contrast to the reactions that produced fertile pyroxene-rich lithologies, these metasomatic processes were probably associated with a low melt/rock ratio. During low melt/rock ratio interactions MgO and Cr_2O_3 contents in clinopyroxene should be buffered by peridotite rather than by infiltrating melts. This can explain why clinopyroxenes from metasomatic pockets and symplectites have high metasomatic components (Al, Ti and Na_2O), along with very high Mg#s that are comparable to those of interstitial residual clinopyroxene.

The foregoing discussion offers textural and compositional evidence that the secondary assemblages found in ESLM xenoliths represent products of mantle metasomatism. Textural and mineral compositional characteristics indicate the role of the following reaction: opx + Cr-rich sp ±phlogopite + Si-undersaturated alkaline melt = Ti-Al-cpx + Ti-rich spinel ± olivine ± other minor phases. However, this reaction should be taken as oversimplification because it cannot account for all the observed textural assemblages. For instance, the presence of phlogopite relicts implies the role of preexisting metasomatic phases and their subsequent breakdown. There are, however, open questions as regards: (i) if metasomatic phases other than phlogopite had also been present and then entirely decomposed? (ii) was phlogopite (±other phases) related to a compositionally different metasomatic event, and (iii) when (and why?) exactly did breakdown reactions occur? Very high TiO_2 contents found in phlogopite relicts (Cvetković *et al.* 2004 *b*) lend support to the conclusion that the mica was related to compositionally similar metasomatic agents. Amphibole can be a likely candidate to have been originally present together with phlogopite and this possibility is further discussed below. However, to constrain the exact time and cause of the breakdown reactions is very difficult, if not impossible. Generally, it could have occurred within the mantle due to thermal(± new infiltration) events subsequent to the main enrichment phase or it might have been related to post-entrainment decompression melting due to the fast uplift of host lavas.

Consequently, a more general conclusion derived from this section is that the ESLM has undergone addition of a silica-undersaturated alkaline melt rich in Fe-Ti-Al, REE, HFSE and CO_2 and H_2O. Similar metasomatic evidence has been known from many xenolith suites and peridotite massifs and was also interpreted in terms of carbonate-rich alkaline silicate metasomatism (e.g. Harte 1987; Canil & Scarfe 1989; McGuire & Mukasa 1997; Wilshire 1987; Xu *et al.* 1996; Witt Eickschen & Kramm 1998; Delpech *et al.* 2004, Rivalenti *et al.* 2004, etc.).

Implications from the geochemistry of host basanites

Presented textural and mineral chemistry evidence suggests that prior to the onset of the Paleogene mafic alkaline magmatism the ESLM already contained metasomatized domains. If this is correct, it raises a logical question: could these metasomatized lithospheric

regions have played any role in petrogenesis of the host basanites? In this section we try to demonstrate that this is a likely hypothesis, namely that the host lavas could have originated by melting of a mantle source containing metasomatic assemblages similar to those observed in xenoliths.

We have used the following two-fold approach: (a) performing inversion modeling based on the whole-rock trace element data of basanites adopting the method of Cebria and Lopez-Ruiz (1996) for constraining the source composition and bulk partition coefficients of incompatible elements during the partial melting, and (b) inferring possible mineralogical characteristics of the source and comparing them to the observed mineralogy of metasomatic associations found in xenoliths. As mentioned above, for the modeling we used the Sokobanja basanites because their composition appears to be unaffected by fractionation and contamination processes and because they have the most uniform isotopic composition of all the East Serbian Paleogene alkaline rocks.

The analyses used for modeling, general explanation of the procedure and the used equations are given in Appendix, while the step-by-step modeling procedure can be found in Cebria and Lopez-Ruiz (1996). The results of the modeling are presented in Table 4. The modeled source is enriched in highly and moderately incompatible elements (e.g. average estimates between ~35-40xchondrite for U-Th-Nb-Ta to around 2xchondrite for HREE). The trace element pattern of the source is compared to the pattern of the MORB source (Salters and Stracke, 2004) in Figure 9. With respect to the MORB-source, the calculated source is more than two orders of magnitude enriched in concentrations of highly incompatible and two to one orders of magnitude in contents of highly to moderate incompatible elements. The concentrations in the range Dy-Lu are either very similar or slightly lower in comparison to the MORB-source.

The results of the modeling imply that the primary magmas of Sokobanja basanites were not derived by melting of a homogeneous asthenospheric source, provided that it is MORB-like. Even extremely small degrees of partial melting (<<1 %) are not capable of producing the observed enrichment in most incompatible elements. Partial melting of deep mantle (plume) sources can be excluded as there is no geological evidence that mantle plume could have been related to the petrogenesis of East Serbian Paleogene alkaline rocks (e.g. Cvetković *et al.* 2004 *a*). Cvetković *et al.* (2005) performed partial melting modeling using the approach of McKenzie and O'Nions (1995). The model involving 5-10 % of melting of a garnet- and amphibole-bearing REE-enriched mantle (MORB-source enriched by 8% of melts formed by extraction of 0.3 % of fractional melting of the same source) could roughly reproduce the observed REE patterns, but still had difficulties to match the observed concentrations of La and Ce. Importantly, the model did not take into consideration Sr and HFSE contents, which are generally very high in alkali basalts.

The modeling presented here has an advantage in determining not only the trace element concentrations in the source but also their bulk distribution coeffecients. These can be used as additional constraints on the source mineralogy. The estimated ranges of bulk partition coefficients for the source phases (D_0) and for the phases entering the melt (P_L) are also given in Table 4. The obtained D_0 values confirmed that La and Ce (D_0 ~0.002) behaved most incompatibly during partial melting. This was inferred from co-variation diagrams and was used as a pre-assumption in the modeling (see Appendix). D_0 values for Nd (~0.007) and Th (~0.009) suggest slightly more compatible behavior of these two elements. All other trace elements show D_0 >0.02. P_2O_5 and Sr are least incompatible elements with average D_0 values

of 0.063 and 0.07, respectively. Among the incompatible elements only Ti behaved more compatibly but due to very poor correlation ($r_{[La\ vs\ TiO2]}$~0.2) it was excluded from the modeling. K, Rb and Ba were also excluded from the modeling because of their near compatible behavior. This characteristic is observed in most alkaline provinces and was usually attributed to the presence of amphibole and/or phlogopite in the source (e.g. Wilson and Downes, 1991).

To infer possible source mineralogy of the host basanites we compared D_0 values of the basanitic mantle source obtained by inversion modeling with the D_0 values of mantle lithologies differing in their mineral composition using mineral-melt partition coefficients from literature. The results are illustrated in Figure 10 and mineral-melt partition coefficients used in calculations are given in Table 5. Note that the mineralogy of unmetasomatized mantle (shaded area, shown in all diagrams) can roughly reproduce the D_0 values obtained by inversion modeling for the REE (except for Sm, at certain extent) and for Y. On the other hand, there is strong discrepancy in D_0 values for Th, U, Nb, Ta, Sr, P, Zr and Hf, which appear to be much more compatible in the source calculated by the modeling. Consequently, if a metasomatic assemblage was present in the source of Sokobanja basanites, which is indeed our hypothesis, it must be an association which can substantially increase D_0 for the mentioned elements without affecting bulk partition coefficients for REEs. Amphibole524 bearing metasomatized mantle (with or without phlogopite) is characterized by very high $_{REE}D_0$ but the D_0 values for Nb, Ta, Sr and P are still too low (Figure 10b,c). The presence of phlogopite alone is also unable to account for high D_0 for Nb, Ta, Sr and P (Figure 10d). The best fit with D_0 of the calculated basanitic source was produced using anhydrous metasomatized mantle with small additions of metasomatic clinopyroxene and carbonate (~5 %) and with traces of ilmenite (~1 %) and apatite (~0.05 %) (Figure 10e). The pattern of D_0 values is almost completely matched along with still higher $_{U}D_0$ and $_{LREE}D_0$ (x0.5-x4) than in the mantle source calculated by the inversion technique. Note that any addition of phlogopite and especially amphibole will produce an increase in $_{LREE}D_0$ and thereby a larger misfit with the pattern of the modeling.

The presented modeling strongly depends on mineral-melt partition used and for some mineral/element pairs these values have a wide range or are poorly constrained, or both and for these reasons this should be taken as an indication rather than as a straightforward conclusion. However, the shown modeling strongly argues that the presence of minerals found in xenolith-related metasomatic associations is required. Hence, we may assume that the presence of carbonate and apatite in the source of host rocks is a robust hypothesis. In the absence of carbonate the calculated $_{Sr}D_0$ of 0.073 can be matched only if relatively large proportions (>15 %vol) of amphibole are present. However, as shown above, this would make the middle rare-earth elements (Sm-Dy) four to five times more compatible than calculated. If we theoretically assume much lower $_{REE}D_{Amph}$ we would potentially solve the problem of D_0 values in the source. However, even if amphibole enters the melt totally, it cannot account for the $_{Sr}P_L$>0.2 estimated by inversion calculations. On the other hand, because of their high K_{DSr}, traces of carbonate and apatite in the mantle could account for the calculated low $_{Sr}D_0$ and relatively high $_{Sr}P_L$. This conclusion is in accordance with the observation that Mg548 bearing calcite and apatite are frequently found in metasomatic associations found in ESLM xenoliths (also Cvetković *et al.* 2007b). Similar reasoning can be followed to infer the presence of Fe-Ti-oxides as repositories of Nb and Ta, whose estimated concentration in the source is >35xchondrite. Ilmenite is observed in many metasomatic associations in ESLM

xenoliths and this mineral has high partition coefficients for Nb and Ta (e.g. Zack & Brumm 1998). Hence, it can account for high Nb and Ta concentrations in the source and also for their relatively high partitioning into the melt.

Asthenosphere-lithosphere interaction: the order of events

The foregoing discussion implies that there is an agreement in mineral composition, at least qualitatively, between the observed secondary assemblages in the studied xenoliths with inferred metasomatic phases in the source of host magmas. We do not suggest that the metasomatized ESLM xenoliths represent the very source for host magmas. We propose that they may represent counterparts of similar metasomatic regions situated deeper in the lithosphere. In Figure 11 we offer a schematic two-phase model of metasomatic processes that might have occurred at the base of the ESLM. The first phase (Figure 11, A) involves percolation of CO_2 and H_2O-rich mafic alkaline melts and precipitation of primary metasomatic assemblages containing phlogopite and amphibole (Figure 11, A1). The original presence of amphibole may be arbitrary because no amphibole is found in the studied xenoliths. In spite of this fact, amphibole is included in the model mainly because it was found in many other xenolith suites (e.g. Witt-Eickschen *et al.* 1998) and its role in the source processes of alkali basalts and basanites has already been reported by many studies (Jung *et al.* 1998, 2000). The percolation/infiltration processes were most probably facilitated by local deformation and fault zones, along which textural assemblages characterized by rotated, disrupted and partially resorbed spinel grains formed (Figure 11, A2). Simultaneously, small portions of the alkaline melt were trapped by wallrock peridotite and solidified as metasomatic symplectites (Figure 11, A3). The second phase of the model is related to the uplift of hot asthenospheric mantle and this should have occurred at the very onset of the host basanitic magmatism. The asthenospheric uplift produced an increase of heat flow and caused a temperature rise at the base of the lithosphere. Before the uprise, convective mantle reached a critical level and gave rise to partial melting in the source region of basanites (hatched area), decompression and high temperature (along with infiltration of new metasomatic melts?) had caused breakdown of previously formed phlogopite and amphibole. The decomposition of the H_2O-bearing phases left behind anhydrous metasomatic associations (Figure 11, B1), which are texturally and compositionally similar to the assemblages found in the ESLM xenoliths. However, it cannot be excluded that during the capture of xenoliths and shortly after, the metasomatic assemblages might have undergone a new episode of melting and subsequent quenching.

This model uses a general idea of many studies which have linked intraplate alkaline magmatism to lithospheric mantle sources enriched by melts derived from sub-lithospheric convecting mantle at some time in the past (Stein & Hofmann 1992; Baker *et al.* 1998; Beccaluva *et al*., 2001; Bonadiman *et al.*, 2001; Jung *et al.* 2005; Coltorti *et al.* 2004). We have presented evidence of Nb-Ta enrichment in the ESLM and in agreement with Pilet *et al.* (2004) who attributed high Nb and Ta concentrations to short-term metasomatic events in the lithospheric mantle. The model also suggests that the host basanites probably originate from an anhydrous metasomatized peridotite source and that the phlogopite/amphibole signature in these rocks is due to a previous phase of dehydration which occurred prior to magmatism. Assuming an open system, it can be expected that after dehydration, the source was depleted in H_2O, Rb and K with respect to other incompatible elements, especially HFSE. This scenario may be of significance for petrogenesis of at least some alkaline mafic rocks. Similar

idea was very recently reported and modeled by Weinstein *et al.* (2006) on the example of Harrat As Shaam basanites in Israel.

Conclusions

Prior to the onset of the Paleogene mafic alkaline magmatism the East Serbian mantle was already metasomatized. The metasomatism produced domains that are represented by fertile xenoliths and small-scale metasomatic associations found in depleted xenoliths. The composition of the fertile xenoliths is modeled by addition of 5-20 wt% of a basanitic melt to a refractory mantle. The presented model suggests that this lithology could have originated by refertilization of residual mantle regions by relatively Fe-rich alkaline basaltic melts. The small-scale metasomatic associations comprise metasomatic phases crystallized in an open space, those formed due to simultaneous deformation events, and rare symplectitic assemblages. They all show similar mineral composition and imply the role of the following reaction: opx + Cr-rich sp ±phlogopite + Si-undersaturated alkaline melt = Ti-Al-cpx + Ti-rich spinel ± olivine ± other minor phases.

There is an agreement in modal composition, at least qualitatively, between the observed secondary metasomatic assemblages in the studied xenoliths and the source of host magmas, the latter being inferred from inversion modeling. In this context, the host Sokobanja basanites probably originated from a peridotitic source, which contained metasomatic domains similar to those observed in xenoliths. The phlogopite/amphibole signature in these rocks is probably due to a dehydration phase due to further asthenospheric uplift which occurred prior to alkaline magmatism.

This study is supported by Austrian Science Foundation FWF as a Lise Meitner Project No M832-N10 granted to V. Cvetković. The Serbian Ministry of Science and Environmental Protection, Project No 146013 is acknowledged.

References

Anderson, A. T. & Greenland, L. P. 1969. Phosphorous fractionation diagrams as a quantitative indicator of crystallization differentiation of basaltic liquids. *Geochimica et Cosmochimica Acta,* **33,** 493-505.

Aoki, K. & Kushiro, I. 1968. Some clinopyroxenes from ultramafic inclusions in Dreiser Weiher, Eifel. *Contributions to Mineralogy and Petrology,* **25,** 284 –288.

Baker, J., Chazot, G., Menzies, M. & Thirlwall, M. 1998. Metasomatism of the shallow mantle beneath Yemen by the Afar Plume; implications for mantle plumes, flood volcanism, and intraplate volcanism. *Geology (Boulder),* **26** (5)**,** 431-434.

Bea, F., Pereira, M. D. & Stroh, A. 1994. Mineral/leucosome trace-element partitioning in a peraluminous migmatite (a laser ablation-ICP-MS study). *Chemical Geology*, **117,** 291-312.

Beccaluva, L., Bonadiman, C., Coltorti, M., Salvini, L. & Siena, F. 2001. Depletion Events, Nature of Metasomatizing Agent and Timing of Enrichment Processes in Lithospheric Mantle Xenoliths from the Veneto Volcanic Province**.** *J. Petrology*, **42**, 173-188;

Bonadiman C., Coltorti M., Milani L., Salvini L., Siena F. & Tassinari R. 2001. Metasomatism in the lithospheric mantle and its relationships to magmatism in the Veneto Volcanic Province, Italy. *Peridico di Mineralogia*, **LXX/3**, 333-357

Brizi E., Nazzareni, S., Princivalle, F. & Zanazzi, P. F. 2003. Clinopyroxenes from mantle649 related xenocrysts in alkaline basalts from Hannuoba (China): augite-pigeonite

exsolutions and their thermal significance. *Contributions to Mineralogy and Petrology*, **145**, 578-584.
Canil, D. & Scarfe, C. M. 1989. Origin of phlogopite in mantle xenoliths from Kostal Lake Wells Grey Park, British Columbia. *Journal of Petrology,* **30,** 1159-1179.
Carpenter, R. L., Edgar, A. D. & Thibault, Y. 2002) Origin of spongy textures in clinopyroxene and spinel from mantle xenoliths, Hessian Depression, Germany. *Mineralogy and Petrology*, **74**, 149-162.
Cebria, J. M. &. Lopez R. J. 1996. A refined method for trace element modelling of nonmodal batch partial melting processes; the Cenozoic continental volcanism of Calatrava, central Spain. *Geochimica et Cosmochimica Acta*, **60** (8), 1355-1366.
Chazot, G., Menzies, M. A. & Harte, B. 1996. Determination of partition coefficients between apatite, clinopyroxene, amphibole, and melt in natural spinel lherzolites from Yemen: Implications for wet melting of the lithospheric mantle. *Geochimica et Cosmochimica Acta,* **60** (3), 423-437.
Clague, D. A. & Frey, F. A. 1982. Petrology and trace element geochemistry of the Honolulu volcanics, Oahu: Implications for the oceanic mantle below Hawaii. *Journal of Petrology*, **23**, 447-504.
Coltorti M., Bonadiman, C., Hinton, R.W., Siena, F. & Upton, B.G.J. 1999. Carbonatite metasomatism of the oceanic upper mantle: evidence from clinopyroxenes and glasses in ultramafic xenoliths of Grande Comore, Indian Ocean. *Journal of Petrology*, **40**,133–165.
Coltorti, M., Beccaluva, L., Bonadiman, C., Faccini, F., Ntaflos, T. & Siena, F. 2004. Amphibole genesis via metasomatic reaction with clinopyroxene in mantle xenoliths from Victoria Land, Antarctica. *Lithos*, **75**, 115-139.
Cvetković, V., Downes, H., Prelević, D., Jovanović, M. & Lazarov, M. 2004a. Characteristics of the lithospheric mantle beneath east Serbia inferred from ultramafic xenoliths in Palaeogene basanites. *Contributions to Mineralogy and Petrology,* **148** (3)**,** 335-357.
Cvetković, V., Prelević, D., Downes, H., Jovanović, M., Vaselli, O. & Pecskay, Z. 2004b. Origin and geodynamic significance of Tertiary postcollisional basaltic magmatism in Serbia (central Balkan Peninsula). *Lithos,* **73,** 161-186.
Cvetković, V., Höck, V. & Prelević, D. 2005. Mantle source characteristics of the Paleogene mafic alkaline rocks of the East Serbian Carpatho-Balkanides. *Mitt. Österr. Miner. Ges.* ***151****,* 36.
Cvetković, V., Downes, H., Prelević, D., Lazarov, M. & Resimić-Sarić, K. 2007a. Geodynamic significance of ultramafic xenoliths from Eastern Serbia: Relics of sub-arc oceanic mantle? *Journal of Geodynamics,* **43**, 504-527.
Cvetković, V., Lazarov, M., Downes, H. & Prelević, D. 2007b. Modification of the subcontinental mantle beneath East Serbia: Evidence from orthopyroxene-rich xenoliths. *Lithos,* **94**, 90-110.
Dal Negro, A., Manoli, S., Secco, L. & Piccirillo, E. M. 1989. Megacrystic clinopyroxenes from Victoria (Australia): crystal chemical comparisons of pyroxenes from high and low pressure regimes. *European Journal of Mineralogy,* **1,** 105 –121
Dawson, J. B. 1984. Carbonate tuff cones in northern Tanganyika. *Geological Magazine,* **101,** 129-137.
Dawson, J. B. 2002. Metasomatism and partial melting in upper-mantle peridotite xenoliths from the Lashaine Volcano, northern Tanzania. *Journal of Petrology*, **43** (9)**,** 1749-1777.

Delpech, G., Gregoire, M., O'Reilly, S. Y., Cottin, J. Y., Moine, B., MIchon, G. & Giret, A. 2004. Feldspar from carbonate-rich silicate metasomatism in the shallow oceanic mantle under Kerguelen Islands (South Indian Ocean). *Lithos,* **75,** 209-237.
Dobosi, G., Downes, H., Embey-Isztin, A. & Jenner, G. A. 2003. Origin of megacrysts and pyroxenite xenoliths from the Pliocene alkali basalts of the Pannonian Basin (Hungary). *Neues Jahrbuch fur Mineralogie-Abhandlungen,* **178,** 217-237.
Dobosi, G. & Jenner G. J. 1999. Petrologic implications of trace element variation in clinopyroxene megacrysts from the Nógrád volcanic province, north Hungary: a study by laser ablation microprobe–inductively coupled plasma-mass spectrometry. *Lithos,* **46,** 731-749.
Falus, G., Drury, M. R., Van Roermund, H. L. M. & Szabo, C. S. 2004. Magmatism-related localized deformation in the mantle: a case study. *Contributions to Mineralogy and Petrology,* **146,** 493-505.
Foley, S. F., Jackson, S. E., Fryer, B. J., Greenough, J. D. & Jenner, G. A. 1996. Trace element partition coefficients for clinopyroxene and phlogopite in an alkaline lamprophyre from Newfoundland by LAM-ICP-MS. *Geochimica et Cosmochimica Acta,* **60** (4)**,** 629-638.
Fujimaki, H. 1986. Partition-Coefficients of Hf, Zr, and Ree between Zircon, Apatite, and Liquid. *Contributions to Mineralogy and Petrology,* **94** (1)**,** 42-45.
Fujimaki, H., Tatsumoto, M. & Aoki, K.-i. 1984. Partition coefficients of Hf, Zr, and REE between phenocrysts and groundmasses. *Journal of Geophysical Research,* **89,** 662-672.
Ghiorso, M. S. & Carmichael, I. S. E. 1987. Modeling magmatic systems: Petrologic applications. *Reviews in Mineralogy,* **17,** 467–499.
Gorring, M. L. & Kay, S. M. 2000. Carbonatite metasomatized peridotite xenoliths from suthern Patagonia: implications for lithospheric processes and Neogene plateau magmatism. *Contributions to Mineralogy and Petrology,* **140,** 55-72.
Gregoire, M., Moine, B. N., O'Reilly, S. Y., Cottin, J. Y. & Giret, A. 2000. Trace element residence and partitioning in mantle xenoliths metasomatized by highly alkaline, silicate-and carbonate-rich melts (Kerguelen Islands,Indian Ocean). *Journal of Petrology,* **41,** 477 –509.
Green, T. H., Adam, J. & Site, S. H. 1993. Proton microprobe determined trace element partition coefficients between pargasite, augite and silicate or carbonatitic melts. *EOS,* **74,** 340.
Hart, S. R. 1984. A large scale isotope anomaly in the southern hemisphere mantle. *Nature,* **309,** 753–757
Harte, B. 1987. Metasomatic events recorded in mantle xenoliths: An overview. *In:* Nixon, P. (ed.) *Mantle Xenoliths.* John Wiley, Hoboken, N. J., 625-640.
Horn, I., Foley, S. F., Jackson, S. E. & Jenner, G. A. 1994. Experimentally determined partitioning of high field strength- and selected transition elements between spinel and basaltic melt. *Chemical Geology,* **117,** 193-218.
Ionov, D. A., Gregoire, M. & Prikhod'ko, V.S. 1999. Feldspar-Ti-oxide metasomatism in off737 cratonic continental and oceanic upper mantle. *Earth and Planetary Science Letters,* **165 (1)**: 37-44.
Ionov, D. & Harmer, R. E. 2002. Trace element distribution in calcite-dolomite carbonatites from Spitskop: inferences for differentiation of carbonatite magmas and the origin of carbonates in mantle xenoliths. *Earth and Planetary Science Letters,* **198,** 495-510.

Ionov, D., Hofmann, A. W. & Shimizu, N. 1994. Metasomatism-induced Melting in Mantle Xenoliths from Mongolia. *Journal of Petrology,* **35** (3)**,** 753-785.
Irving, A. J. 1974. Megacrysts from the Newer Basalts and other basaltic rocks of southern Australia. *Bulletin of the Seismological Society of America,* **85,** 1503-1514.
Jovanović, M., Downes, H., Vaselli, O., Cvetković, V., Prelević, D. & Pecskay, Z. 2001. Paleogene mafic alkaline volcanic rocks of East Serbia. *Acta vulcanologica,* **13**(1-2)**,** 159-173.
Jung, S. & Masberg, P. 1998. Major- and trace-element systematics and isotope geochemistry of Cenozoic mafic volcanic rocks from the Vogelsberg (central Germany); constraints on the origin of continental alkaline and tholeiitic basalts and their mantle sources. *Journal of Volcanology and Geothermal Research,* **86** (1-4)**,** 151-177.
Jung, S. & Hoernes, S. 2000. The major- and trace-element and isotope (Sr, Nd, O) geochemistry of Cenozoic alkaline rift-type volcanic rocks from the Rhoen area (central Germany): petrology, mantle source characteristics and implications for asthenosphere756 lithosphere interactions. *Journal of Volcanology and Geothermal Research,* **99** (1-4)**,** 27-53.
Jung, S., Pfaender, J. A., Bruegmann, G. & Stracke, A. 2005. Sources of primitive alkaline volcanic rocks from the Central European Volcanic Province (Rhoen, Germany) inferred from Hf, Os and Pb isotopes. *Contributions to Mineralogy and Petrology,* **150**, 546-559.
Karner, J. M., Papike, J. J. & Shearer, C. K. 2003. Olivine from planetary basalts; chemic signatures that indicate planetary parentage and those that record igneous setting and process. *American Mineralogist,* **88** (5-6)**,** 806-816.
Kempton, P. D. 1987. Mineralogic and geochemical evidence for differing styles of metasomatism in spinel lherzolite xenoliths: enriched mantle source regions of basalts? *In:* Menzies M. A. & Hawkesworth C. J. (eds) *Mantle metasomatism*. Academic Press Inc., London, 45-89.
Kepezhinskas, P. K., Defant, M. J. & Drummond, M. S. 1995. Na Metasomatism in the Island-Arc Mantle by Slab Melt-Peridotite Interaction: Evidence from Mantle Xenoliths in the North Kamchatka Arc. *Journal of Petrology,* **36** (6)**,** 1505-1527.
Kepezhinskas, P. K., Defant, M. J. & Drummond, M. S. 1996. Progressive enrichment of island arc mantle by melt peridotite interaction inferred from Kamchatka xenoliths. *Geochemica et Cosmochimica Acta,* **60,** 1217-1229.
Keshav S., Corgne A., Gudfinnsson G. H., Bizimis M., McDonough W. F. & Fei Y. W. 2005. Kimberlite petrogenesis; insights from clinopyroxene-melt partitioning experiments at 6 GPa in the CaO-MgO-Al (sub 2) O (sub 3) -SiO (sub 2) -CO (sub 2) system. *Geochimica et Cosmochimica Acta,* **69** (11)**,** 2829-2845.
Kluegel, A. 1998. Reactions between mantle xenoliths and host magma beneath La Palma (Canary Islands); constraints on magma ascent rates and crustal reservoirs. *Contributions to Mineralogy and Petrology,* **131** (2-3)**,** 237-257.
Larsen, L. M., Pedersen, A. K., Sundvoll, B. & Frei, R. 2003. Alkali picrites formed by melting of old metasomatized lithospheric mantle: Mantdlat Member, Vaigat Formation, Palaeocene of West Green-land. *Journal of Petrology,* **44,** 3–38.
Latourrette, T., Hervig, R. L. & Holloway, J. R. 1995. Trace-Element Partitioning between Amphibole, Phlogopite, and Basanite Melt. *Earth and Planetary Science Letters,* **135** (1-4)**,** 13-30.
Luhr, J. F., Carmichael, I. S. E. & Varekamp, J. C. 1984. The 1982 eruptions of El Chichon

volcano, Chiapas, Mexico: mineralogy and petrology of the anhydrite-bearing pumices. *Journal of Volcanology and Geothermal Research,* **23,** 69-108.
McDonough, W. H. & Frey, F. A. 1989. Rare earth elements in upper mantle rocks. *In*: Lipin, B. R. & McKay, G. A. (eds) *Geochemistry and Mineralogy of Rare Earth Elements, Reviews in Mineralogy.* Mineralogical Society of America, Washington, DC, **21,** 99-145.
Mahood, G. A. & Stimac, J. A. 1990. Trace-element partitioning in pantellerites and trachytes. *Geochimica et Cosmochimica Acta,* **54,** 2257-2276.
McDonough, W. F. & Sun, S.-s. 1995. The composition of the Earth. *Chemical Geology,* **120,** 223-253.
McGuire, A. V. & S. B. Mukasa 1997. Magmatic modification of the uppermost mantle beneath the Basin and Range to Colorado Plateau transition zone; evidence from xenoliths, Wikieup, Arizona. *Contributions to Mineralogy and Petrology,* **128** (1)**,** 52-65.
McKenzie, D. & O'Nions, R. K. 1995. The source regions of ocean island basalts. *Journal of Petrology,* **36** (1)**,** 133-159.
Menzies, M. A., Rodgers, N., Tindle, A. & Hawkesworth, C. J. 1987. Metasomatic and enrichment processes in lithospheric peridotites, and effect of asthenosphere litgosphere interaction. *In:* Menzies, M. A. & Hawkesworth, C. J. (eds) *Mantle Metasomatism.* London: Academic Press, 313-361.
Morishita, T. & Arai, S. 2003. Evolution of spynel pyroxene symplectite in spinel-lherzolites from the Horoman Complex, Japan. *Contributions to Mineralogy and Petrology,* **144,** 509-522.
Neumann, E.-R., Wulff-Pedersen, E., Pearson, N. & Spencer, E. A. 2002. Mantle xenoliths from Tenerife (Canary Islands); evidence for reactions between mantle peridotites and silicic carbonatite melts inducing Ca metasomatism. *Journal of Petrology,* **43** (5)**,** 825-857.
Nicolas, A. 1986. A melt extraction model based on structural studies in mantle peridotites. *Journal of Petrology,* **27,** 999-1022.
O'Reilly, S. Y. & Griffin, W. L. 1988. Mantle metasomatism beneath western Victoria, Australia: I. Metasomatic processes in Cr-diopside lherzolites. *Geochimica et Cosmochimica Acta,* **52,** 433–447.
Paster, T. P., Schauwecker, D. S. & Haskin, L. A. 1974. The behavior of some trace elements during solidification of the Skaergaard layered series. *Geochimica et Cosmochimica Acta,* **38** (10)**,** 1549-1577.
Pilet, S., Hernandez, J., Bussy, F. & Sylvester, P. 2004. Short-term metasomatic control of Nb/ Th ratios in the mantle sources of intraplate basalts. *Geology (Boulder),* **32** (2)**,** 113-116.
Righter, K. & Carmichael, I. S. E. 1993. Mega-xenocrysts in alkali olivine basalts: fragments of disrupted mantle assemblages. *American Mineralogist,* **78,** 1230-1245.
Rivalenti, G., Zanetti, A., Mazzucchelli, M., Vannucci, R., Cingolani, C. A. (2004). Equivocal carbonatite markers in the mantle xenoliths of the Patagonia backarc; the Gobernador Gregores case; Santa Cruz Province, Argentina. *Contributions to Mineralogy and Petrology,* **147** (6)**,** 647-670.
Salters, V. J. M. & Stracke, A. 2004. Composition of the depleted mantle. *Geochemistry, Geophysics, Geosystems,* **5** (5)**,** 1-27.

Schiano, P., Clocchiatti, R., Shimizu, N. C., Maury, R., Jochum, K. P. & Hofmann, A. 2002. Hydrous, silica-rich melts in the sub-arc mantle and their relationship with erupted arc lavas. *Nature,* **377,** 595-600.
Shaw, C. S. J & Eyzaguirre, J. 2000. Origin of megacrysts in the mafic alkaline lavas of the West Eifel volcanic field, Germany. *Lithos,* **50,** 75-95.
Shaw, D. M. 1970. Trace element fractionation during anatexis. *Geochemica Cosmochimica Acta,* **34,** 237-243.
Smith, D. 1977. The origin and interpretation of spinel-pyroxene clusters in peridotite. *Journal of Geology,* **85,** 476-482.
Stein, M. & Hofmann, A. W. 1992. Fossil plume head beneath the Arabian lithosphere? *Earth and Planetary Science Letters,* **114,** 193-209.
Treuil, M. & Joron, J. L. 1975. Utilisation des elements hygromagmatophyles pour la simplification de la modelisation quantitative des processus magmatiques. Examples de l' Afar et de la Dorsale medioatlantique. *Soc. Ital. Mineral. Petrol.,* **131,** 125-174.
Ulmer, P. 1989. Partitioning of high field strength elements among olivine, pyroxenes, garnet and calc alkaline picrobasalt: experimental results and an application. International *Journal of Mass Spectrometry and Ion Physics,* 42-47.
Vannucci, R., Bottazzi, P., Wulff-Pedersen, E. & Neumann, E.-R. 1998. Partitioning of REE, Y, Sr, Zr and Ti between clinopyroxene and silicate melts in the mantle under La Palma (Canary Islands); implications for the nature of the metasomatic agents. *Earth and Planetary Science Letters,* **158** (1-2)**,** 39-51.
Villemant, B., Jaffrezic, H., Joron, J. L. & Treuil, M. 1981. Distribution Coefficients of Major and Trace-Elements - Fractional Crystallization in the Alkali Basalt Series of Chaine-Des-Puys (Massif Central, France). *Geochimica et Cosmochimica Acta,* **45** (11)**,** 1997-2016.
Weang, W. & Gasparik, T. 2001. Metasomatic clinopyroxenes in diamonds from Lianing province, China. *Geochimica et Cosmochimica Acta,* **65,** 611-620.
Wedepohl, K. H. & Baumann, A. 1999. Central European Cenozoic plume volcanism with OIB characteristics and indications of a lower mantle source. *Contributions to Mineralogy and Petrology,* **136** (3)**,** 225-239.
Wiechert, U., Ionov, D. A. & Wedepohl, K. H. 1997. Spinel peridotite xenoliths from the Atsagin-Dush Volcano, Dariganga lava plateau, Mongolia; a record of partial melting and cryptic metasomatism in the upper mantle. *Contributions to Mineralogy and Petrology,* **126** (4)**,** 345-364.
Weinstein, Y., Navon, O., Altherr, R. & Stein, M. 2006. The Role of Lithospheric Mantle Heterogeneity in the Generation of Plio-Pleistocene Alkali Basaltic Suites from NW Harrat Ash Shaam (Israel). *Journal of Petrology,* **47** (5)**,** 1017-1050.
Wilshire, H. G. & Kirby, S. H. 1989. Dikes, joints and faulths in the upper mantle. *Tectonophysics,* **161,** 23-31.
Wilshire, H. G. & Shervais, J. W. 1975. Al-Augite and Cr-diopside ultramafic xenoliths in rocks from western United States. *Physics and Chemistry of the Earth,* **9,** 257-272.
Wilshire, H. G. 1987. A model of mantle metasomatism. *In* Moriss, E. M. & Pasteris, J. D. (eds) *Mantle Metasomatism and alkaline magmatism*. Geological Society of America Special Papers, **215,** 47-60.
Wilson, M. & Downes, H. 1991. Tertiary-Quaternary Intra-PLate Magmatism in Europe and its Relationship to Mantle Dynamics. *Journal of Petrology,* **32,** 811-849.

Witt, E. G. & Kramm, U. 1998. Evidence for the multiple stage evolution of the subcontinental lithospheric mantle beneath the Eifel (Germany) from pyroxenite and composite pyroxenite/ peridotite xenoliths. *Contributions to Mineralogy and Petrology,* **131**(2-3)**,** 258-272.
Witt-Eickschen, G., Kaminsky, W., Kramm, U. & Harte, B. 1998. The nature of young vein metasomatism in the lithosphere of the West Eifel (Germany); geochemical and isotopic constraints from composite mantle xenoliths from the Meerfelder Maar. *Journal of Petrology,* **39** (1)**,** 155-185.
Wulff, P. E., Neumann, E.-R., Vannucci, R., Bottazzi, P. & Ottolini, L. 1999. Silicic melts produced by reaction between peridotite and infiltrating basaltic melts: ion probe data on glasses and minerals in veined xenoliths from La Palma, Canary Islands. *Contributions to Mineralogy and Petrology*, **137,** 59-82.
Wulff, P. E., Neumann, E. R. Jensen, B. J. 1996. The upper mantle under La Palma, Canary Islands; formation of Si-K-Na-rich melt and its importance as a metasomatic agent. *Contributions to Mineralogy and Petrology,* **125** (2-3)**,** 113-139.
Xu, Y., Mercier, J.-C. C., Menzies, M., Ross, J. V., Harte, B., Lin, C. & Shi, L. 1996. K-rich glass-bearing wherlite xenoliths from Yitong, Northeastern China: petrological and chemical evidence for mantle metasomatism. *Contributions to Mineralogy and Petrology,* **125,** 406-420.
Yaxley, G. M., Crawford, A. J. & Green, D. H. 1991. Evidence for carbonatite metasomatism in spinel peridotite xenoliths from western Victoria, Australia. *Earth and Planetary Science Letters,* **107** (2)**,** 305-317.
Yaxley, G. M., Green, D. H. & Kamenetsky, V. 1998. Carbonatite metasomatism in the southern Australian lithosphere. *Journal of Petrology,* **39,** 1917-1939.
Zack, T. & Brumm, R. 1998. Ilmenite/liquid partition coefficients of 26 trace elements determined through ilmenite/clinopyroxene partitioning in garnet pyroxene. *In:* Gurney, J. J., Gurney, J. L., Pascoe, M. D. & Richardson, S. H. (eds) *7th International Kimberlite Conference.* Red Roof Design, Cape Town, 986-988.
Zangana, N. A., Downes, H., Thirwall, M. F., Marriner, G. F. & Bea, F. 1999. Geochemical variation on peridotite xenoliths and their constituent clinopyroxenes from Ray Pic (French Massif Central): implications for the composition of the shallow lithospheric mantle. *Chemical Geology,* **153,** 11-35.
Zinngrebe, E. & S. Foley, F. 1995. Metasomatism in mantle xenoliths from Gees, West Eifel, Germany; evidence for the genesis of calc-alkaline glasses and metasomatic Ca915 enrichment. *Contributions to Mineralogy and Petrology,* **122**(1-2)**,** 79-96.

APPENDIX

Inversion modeling

This modeling is based on mathematical expressions which govern geochemical behaviour of trace elements during non-modal partial melting processes (Shaw, 1970):

$$C_L^i = \frac{C_0^i}{D_0^i + F(1 - P_L^i)}$$

$$C_{RS}^i = \frac{C_0^i}{(1-F)}\left[\frac{D_0^i - P_L^i F}{D_0^i + F(1 - P_L^i)}\right]$$

Where:

C_0^i - concentration of the element *i* in the source

C_{RS}^i - concentration of the element *i* in the residual solid

C_L^i - concentration of the element *i* in the partial melt

D_0^i - bulk distribution coefficient of the element *i* for the phases present in the source

P_L^i - bulk distribution coefficient of the element *i* for the phases entering the melt

F - amount of partial melt

It is combined with a graphical procedure of Treuil and Joron (1975) for determination of relative degree of incompatibility of the trace elements using C_L^i-C_L^j and C_L^i-C_L^i/C_L^j diagrams. In the element-ratio diagram, when C_L^i is concentration of the most incompatible and C_L^j concentration of a less incompatible element, the slope (A) and intercept (B) have direct relations to geochemical parameters of partial melting processes, which can be mathematically expressed as:

$$A^j = \frac{D_0^j - D_0^i \dfrac{1 - P_0^j}{1 - P_0^i}}{C_0^j}$$

$$B^j = \frac{C_0^i (1 - P_0^j)}{C_0^j (1 - P_0^i)}$$

In the studied suite of samples lanthanum is the most incompatible element. The values of the slope, intercept and correlation coefficient for La-element and slope and intercept for La-La/element diagrams are given in Appendix/Table 2. The graphical expression of relative incompatibility of the studied trace elements is given in Figure by a diagram displaying ratio of intercept on La-element vs slope on La-ratio diagrams (both recalculated on maximal concentrations) in which origin is La. Using the relation between intercepts on La-ratio diagrams for two elements suggested by Clague and Frey (1982):

$$\frac{B^k}{B^j} = \frac{C_0^j (1 - P_0^k)}{C_0^k (1 - P_0^j)}$$

it was possible to calculate ratios of Ce/La, Ce/Nd, Ce/Th and Ce/Lu and ranges of La, Ce, Nd and Th concentrations, namely their minimal enrichment in the source. Because for the Equation (3) it was necessary to constrain P_L^j and P_L^k values the assumptions that (a) P_L values for Ce, Nd and Th are negligible against 1, which is inferred above, and (b) that the source concentrations of Lu are in range of 2x-4xchondrite as suggested by McDonough & Frey (1989). In addition, using the above constrained minimal concentrations of Ce in the source and the least enriched rock sample with La=54 ppm (to satisfy that $D_0 << F$), maximum degree of partial melting was estimated of F>0.1, by the equation:

$$F = \frac{B^j C_0^j}{C_L^i}$$

The calculation of C_0, D_0 and P_L values for La, Ce, Yb and Lu was performed using a best fit solution of a system of non-linear equations combining Equation (1) and (2) and assuming other constraints used in the initial approach: $F_{max}<0.12$; $D_0^i<P_L^i$; $D_0^{La} \sim D_0^{Ce} \sim 0$; $D_0^{La}<D_0^{Ce}<D_0^{Yb}<D_0^{Lu}$. The combination of the obtained parameters was used to estimate that the maximum percentage of melting is F=0.117. Finally, the C_0, D_0 and P_L for other elements were calculated using the equations:

$$1 - P_L^j = D_0^j \frac{1 - P_L^i}{\frac{A^j}{B^j} C_0^i + D_0^i}$$

$$\frac{C_0^j}{C_L^j} = D_0^j \left[1 + \frac{F(1 - P_L^i)}{\frac{A^j}{B^j} C_0^i + D_0^i} \right],$$

which include the above estimated values for D_0^{La}, P_L^{La}, C_0^{La} and F. The assumptions that $D_0^i<P_L^i$ and that C_{RS}^i must be <0 were satisfied.

FIGURE CAPTIONS

Fig. 1. (a): A plane parallel (PPL) photomicrograph of a clinopyroxene-rich lherzolite; two clinopyroxene crystals with spongy zones are situated within the central part of the image; note different appearance of replacement selvage around the orthopyroxene (upper right), (b): A PPL photomicrograph of a spinel-rich olivine websterite showing a spinel accumulation; the spinel grains form a puzzle-like texture (see also Figure 2); the clinopyroxene and orthopyroxene show spongy zones and replacement selvage, respectively, similar to those seen in A, (c): A back-scattered electrone (BSE) image of a metasomatic pocket in a harzburgite xenolith; the arrows show replacement selvages around orthopyroxene, (d): A BSE image displaying a spinel included in metasomatic clinopyroxene; the spinel shows Ti-rich overgrowth, (e): A BSE image of a coarse-grained spinel with a reaction pattern of increasing Fe-Ti and slightly increasing Cr contents (the analyses 1-5 are shown in Table 2), (f): A BSE image of a rounded pocket with euhedral clinopyroxene and Al-rich spinel which are completely anclosed by Mg-bearing carbonate. Abbreviations: sp – spinel, ol – olivine, opx – orthopyroxene, cpx – clinopyroxene.

Fig. 2. (a): A PPL scanned thin-section image of a slightly sheared harzburgite xenolith; in the right-hand part of the xenolith a spinel- and orthopyroxene-rich zone exists, (b): A BSE image of a detail from A showing a partially disrupted spinel grain, (c, d): BSE images of details from B showing spongy rims of the spinel crystals as well as clinopyroxene and olivine neoblasts, orthopyroxene relicts and altered glass (?) within the reaction assemblage, (e): A BSE image displaying another spinel aggregate with a jig-saw-fit puzzle texture, (f): A BSE image of a detail from E showing a pocket inside a spinel crystal; the pocket contains a perfect apatite crystal as well as subhedral tiny grains of clinoypyroxene and altered olivine all enclosed in a carbonate.

Fig. 3. (a): A BSE image showing a lenticular clinopyroxene-olivine-spinel symplectite found in a Mg-rich dunite xenolith, (b): A BSE image of isolated clinopyroxene-spinel and olivine-spinel intergrowths without having any form of concentrated symplectite aggregates.

Fig. 4. Trace element patterns of clinopyroxene from metasomatic and residual xenolith assemblages. Chondrite and primitive mantle normalization after McDonough & Sun (1995).

Fig. 5. MgO vs Fe_2O_3 diagram for whole rock samples of mafic alkaline rocks of Sokobanja showing the effects of accumulation olivine in the studied samples.

Fig. 6. A simple two-member mixing model based on Al_2O_3 vs CaO/Al_2O_3 and TiO_2 vs CaO/Al_2O_3 variations. It shows that the composition of the fertile xenoliths can be matched by addition of 5-20 % of melt similar to the host basanites to depleted peridotite xenoliths. The whole rock composition was recalculated using mineral chemistry and modal analyses (Cvetković *et al.* 2004 *b*).

Fig. 7. Fe^{3+} (p.f.u.) vs TiO_2 (wt%) for spinel and Fe-Ti-oxide from various mineral associations found in East Serbian xenoliths.

Fig. 8. Mg#(100*MgO/MgO+FeO) vs Al_2O_3 (a), TiO_2 (b), Na_2O (c) and Cr_2O_3 (d) for clinopyroxene from various associations found in East Serbian xenoliths.

Fig. 9. The primitive mantle-normalized trace element pattern showing the source composition inferred from inverse modeling. For comparison is shown the pattern of the source of mid-ocean ridge basalts (MORB, McKenzie & O'Nions 1991).

Fig. 10. A comparison between $D_{mineral/melt}$ values for the source of basanite primary melts obtained by inverse modeling (full squares) with $D_{mineral/melt}$ values for unmetasomatized mantle (shaded area, shown in all diagrams) which is varying in modal composition between depleted mantle (57% olivine, 28% orthopyroxene, 13% clinopyroxene and 2% spinel; Workman & Hart 2005) and average of ESLM depleted xenoliths (74% olivine, 20% orthopyroxene, 4% clinopyroxene and 2% spinel; Cvetković *et al.* 2004) as well as with various modally metasomatized mantle (see the figure for explanation).

Fig. 11. A schematic model of metasomatic processes within the ESLM.

APPENDIX

Figure/Appendix. Diagram of A_j vs B_j displaying relative incompatibility of the studied elements, where: A_j is the slope on La vs La/element(j) diagram and Bj is the intercept on La vs element (j) diagram.

Appendix/Table. *Results of inversion modeling of the source composition of the host basanites; the minimal (MIN), maximal*

	Aj	Bj	r		Aj	Bj
Th	0.156	0.485	0.701	La/Th	0.0067	5.732
U	0.029	0.699	0.757	La/U	0.1224	17.548
Nb	0.958	17.047	0.729	La/Nb	0.0031	0.62
Ta	0.063	0.727	0.780	La/Ta	0.0362	11.158
Ce	1.743	1.340	0.931	La/Ce	0.00002	0.56526
Sr	8.444	437.360	0.862	La/Sr	0.0005	0.0336
Nd	0.671	2.789	0.775	La/Nd	0.001	1.3334
P2O5	0.008	0.329	0.738	La/P2O5	0.5582	43.612
Zr	1.996	55.287	0.720	La/Zr	0.0018	0.233
Hf	0.054	1.027	0.769	La/Hf	0.0557	10.73
Sm	0.102	1.720	0.730	La/Sm	0.0273	6.025
Eu	0.032	0.479	0.930	La/Eu	0.0861	19.896
TiO2	0.006	1.438	0.261	La/TiO2	0.4403	7.1075
Gd	0.071	2.083	0.898	La/Gd	0.0539	6.2438
Tb	0.013	0.182	0.820	La/Tb	0.2045	50.087
Dy	0.062	1.256	0.871	La/Dy	0.0523	8.9451
Y	0.334	6.934	0.773	La/Y	0.0094	1.6603
Ho	0.010	0.335	0.872	La/Ho	0.3972	40.649
Er	0.028	0.780	0.842	La/Er	0.1376	16.355
Tm	0.005	0.064	0.596	La/Tm	0.4837	143.8
Yb	0.023	0.761	0.591	La/Yb	0.1736	17.87
Lu	0.004	0.101	0.754	La/Lu	1.0765	123.93

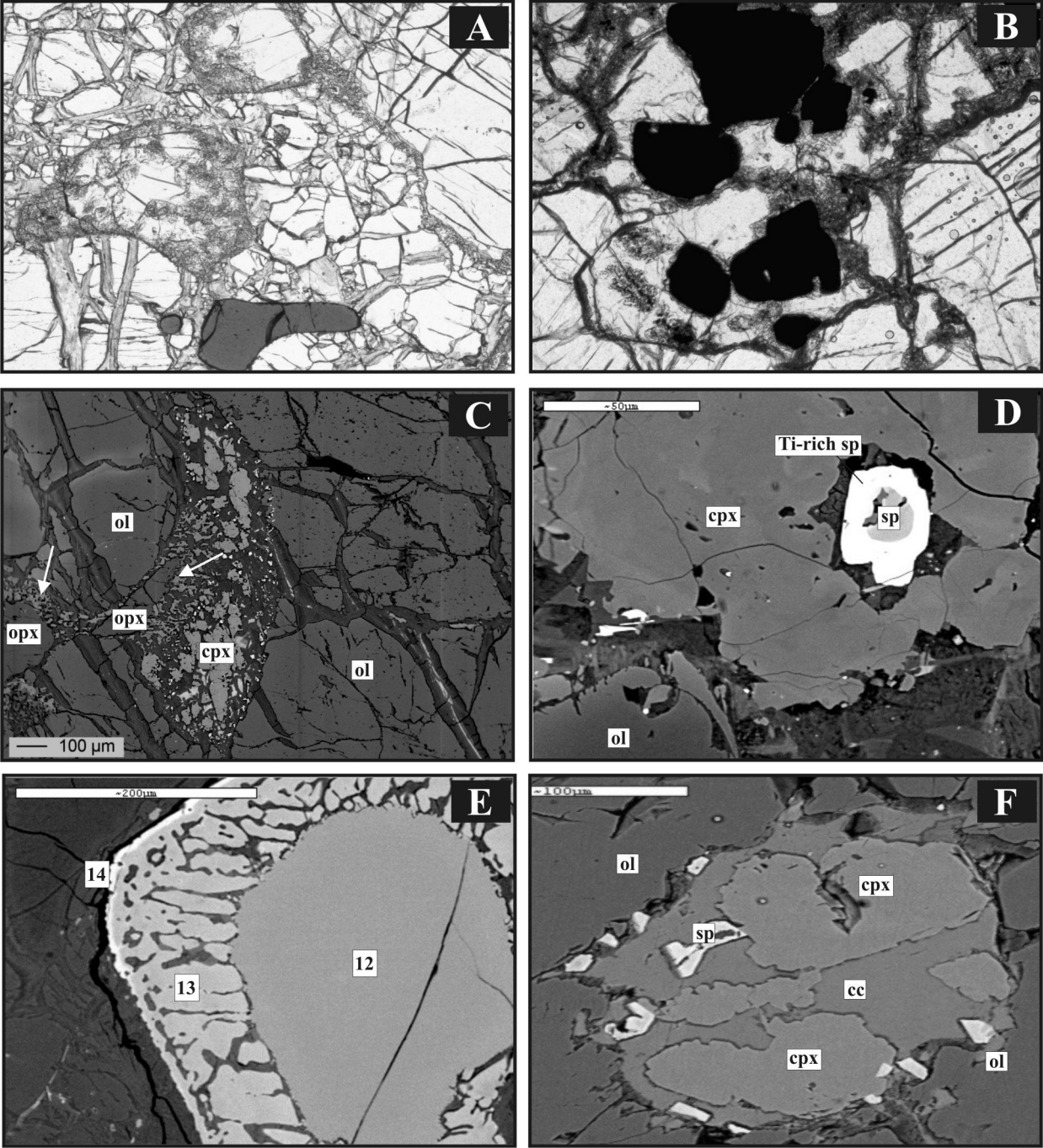
A
B
C
ol
opx
opx
cpx
ol
100 µm
D
~50µm
Ti-rich sp
cpx
sp
ol
E
~200µm
14
12
13
F
~100µm
ol
cpx
sp
cc
cpx
ol

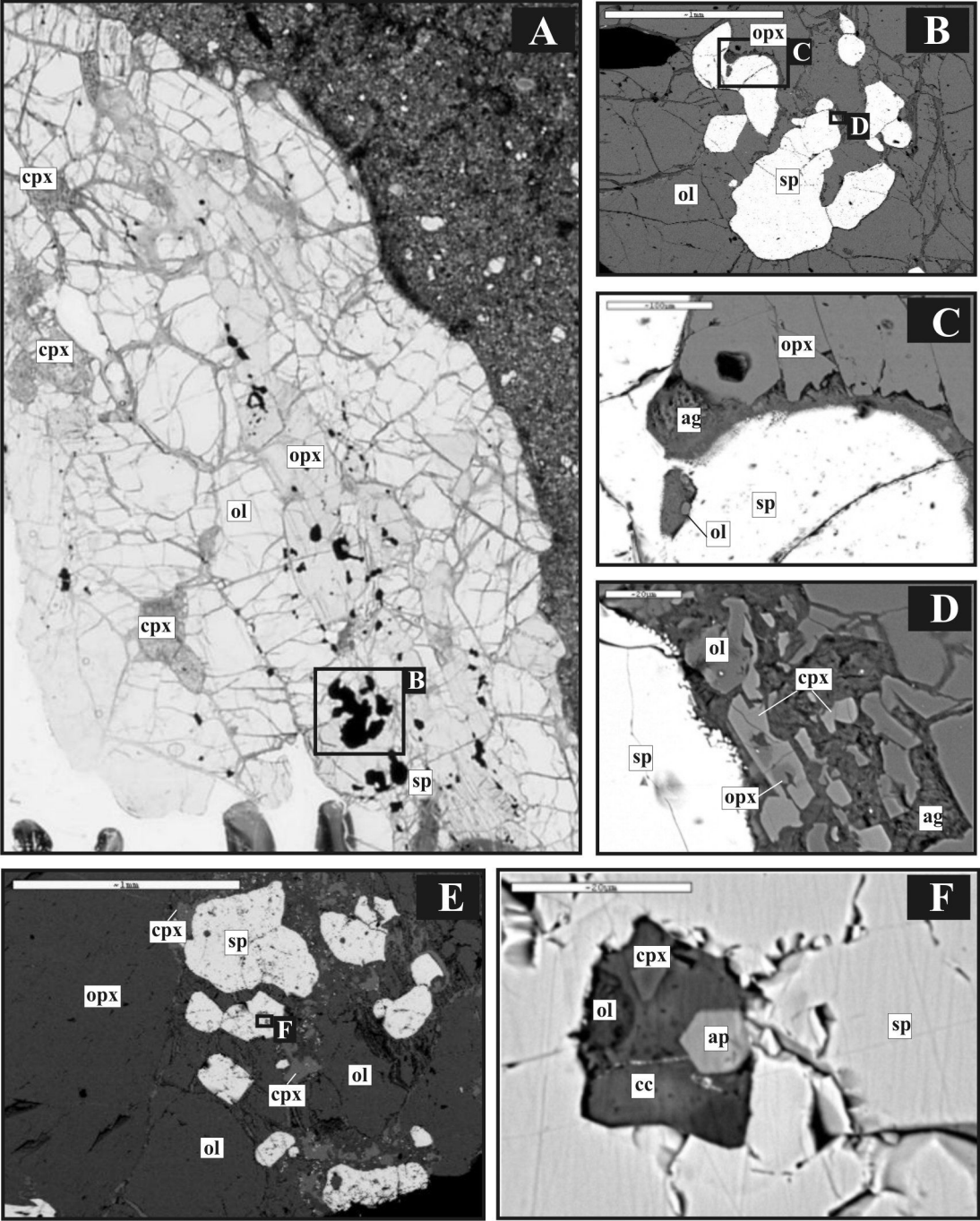
A
cpx
cpx
opx
ol
cpx
B
sp
B
opx
C
D
sp
ol
C
opx
ag
sp
ol
D
ol
cpx
sp
opx
ag
E
cpx
sp
opx
F
ol
cpx
ol
F
cpx
ol
ap
sp
cc

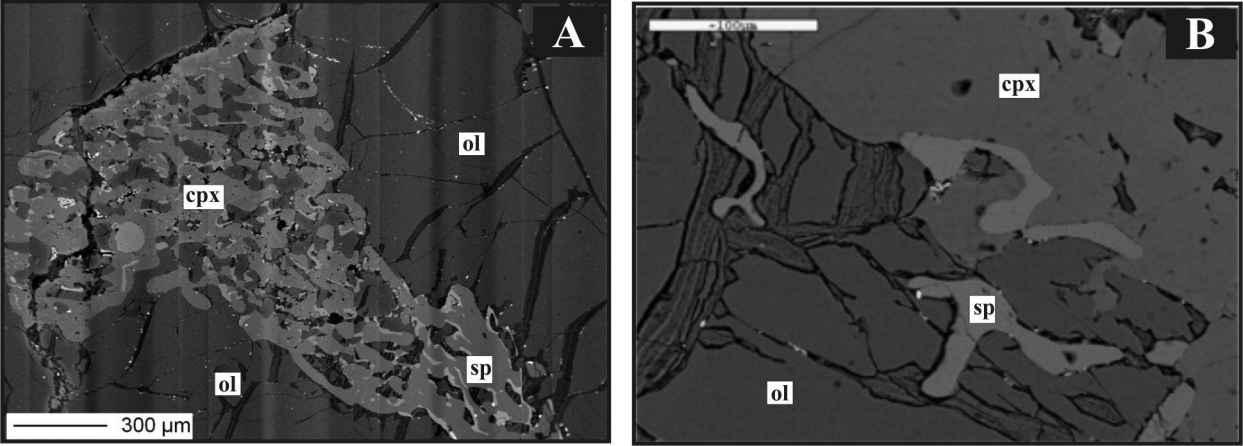
A
ol
cpx
sp
ol
300 µm
B
cpx
sp
ol

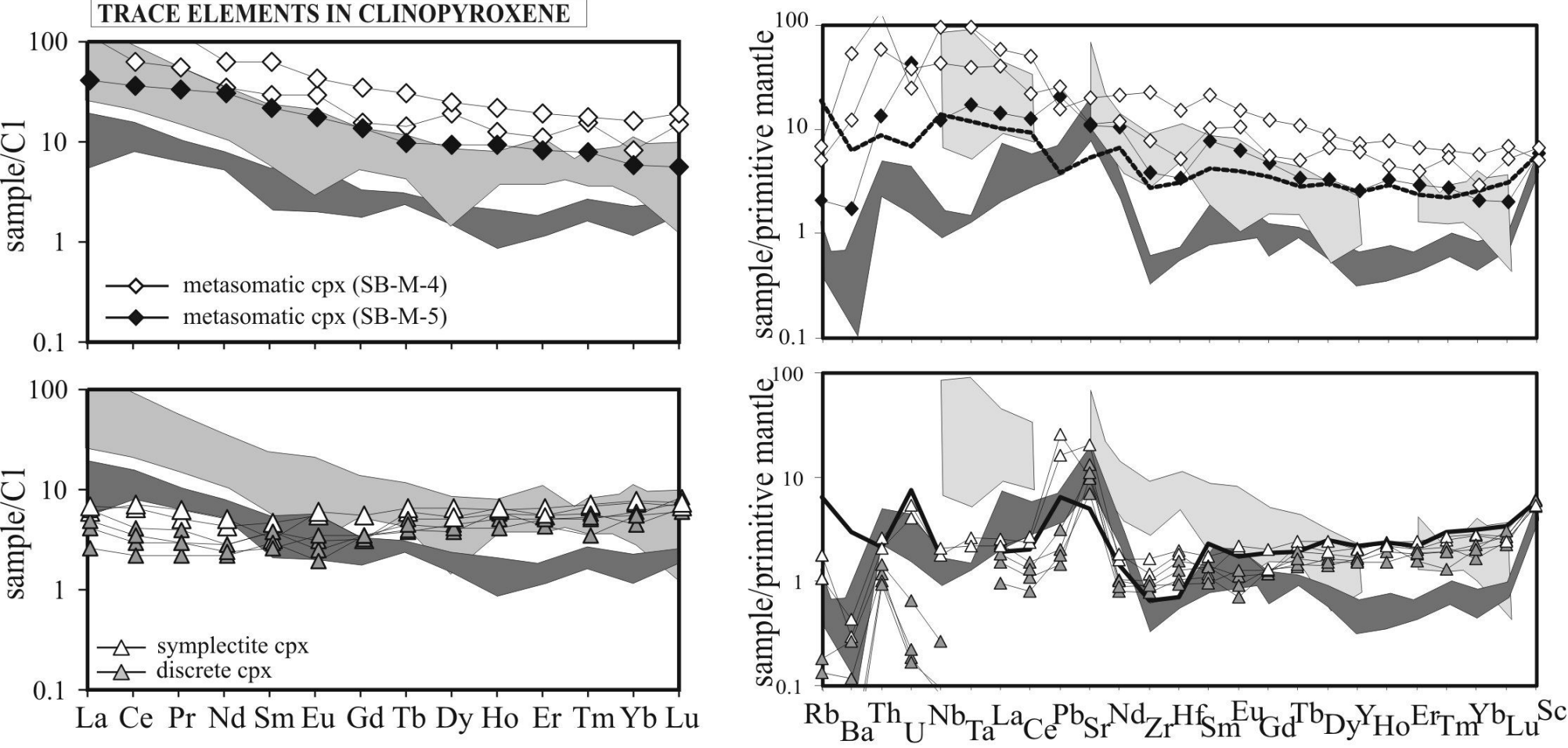
TRACE ELEMENTS IN CLINOPYROXENE
sample/C1
100
10
1
0.1
metasomatic cpx (SB-M-4)
metasomatic cpx (SB-M-5)
symplectite cpx
discrete cpx
La Ce Pr Nd Sm Eu Gd Tb Dy Ho Er Tm Yb Lu
sample/primitive mantle
Rb Ba Th U Nb Ta La Ce Pb Sr Nd Zr Hf Sm Eu Gd Tb Dy Y Ho Er Tm Yb Lu Sc
Metasomatic cpx (Cvetković et al. 2004a)
Residual cpx (Cvetković et al. submitted)
Cpx from orthopyroxene replacements (Cvetković et al. 2006, in press)
Euhedral pocket clinopyroxene (Cvetković et al. submitted)

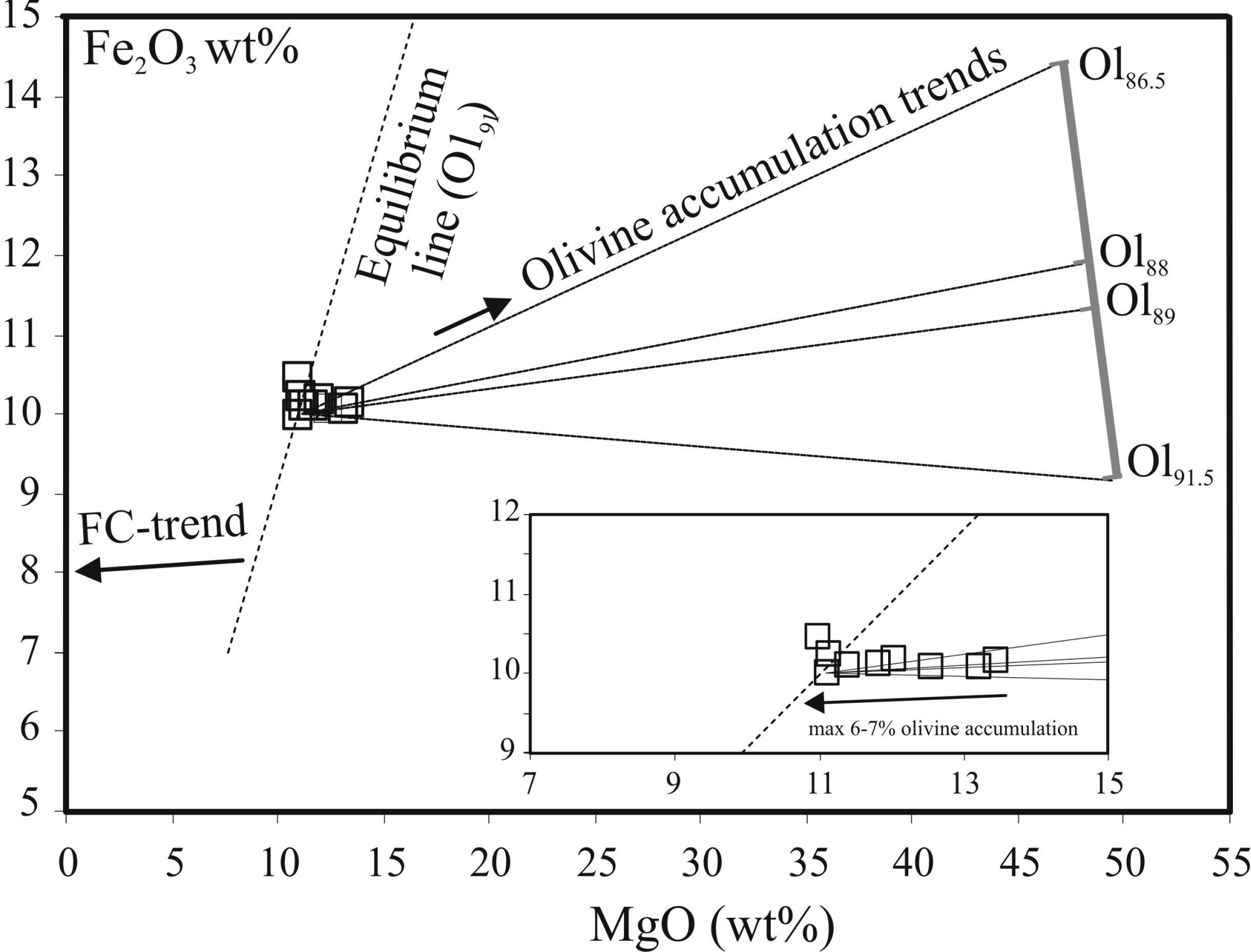
Fe2O3 wt%
Equilibrium line (Ol91)
Olivine accumulation trends
Ol86.5
Ol88
Ol89
Ol91.5
FC-trend
max 6-7% olivine accumulation
MgO (wt%)

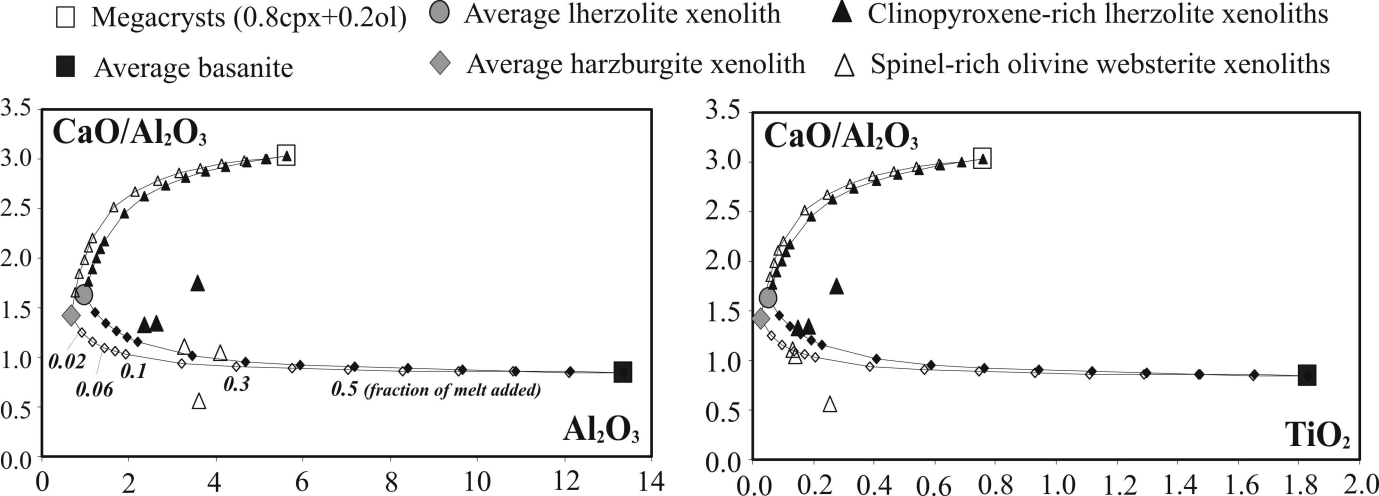
Megacrysts (0.8cpx+0.2ol)
Average lherzolite xenolith
Clinopyroxene-rich lherzolite xenoliths
Average basanite
Average harzburgite xenolith
Spinel-rich olivine websterite xenoliths
CaO/Al2O3
Al2O3
0.02
0.06
0.1
0.3
0.5 (fraction of melt added)
CaO/Al2O3
TiO2

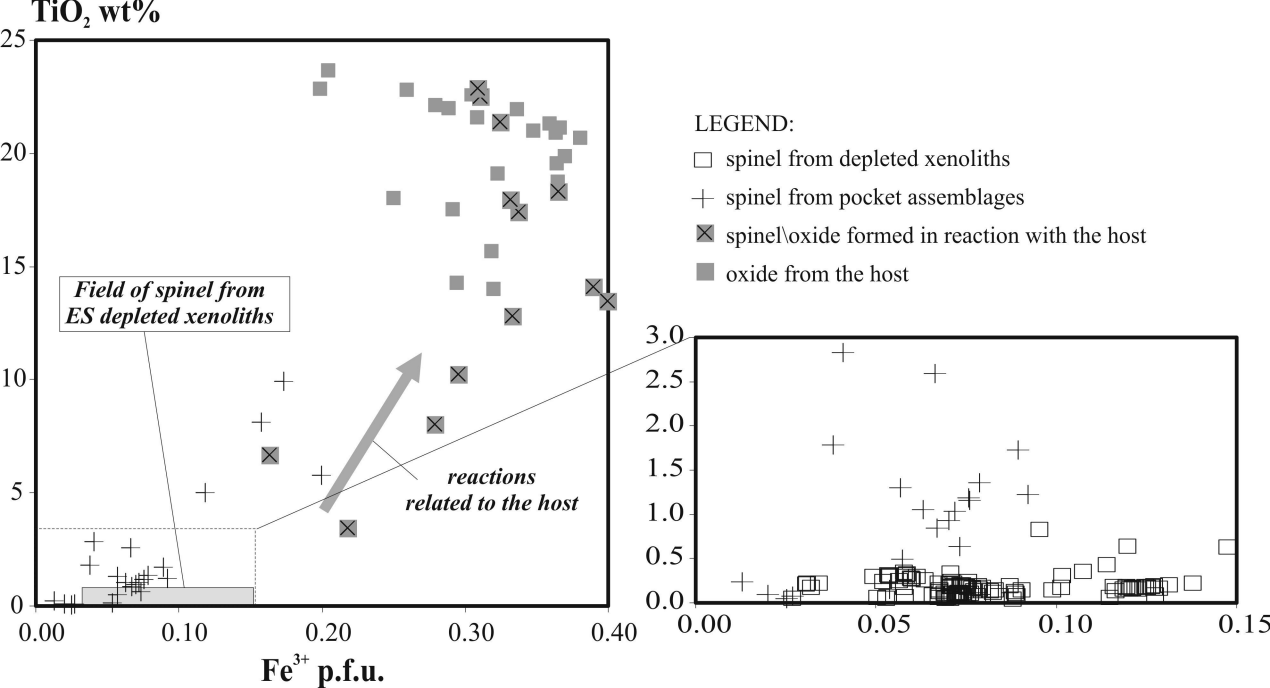
TiO2 wt%
25
20
15
10
5
0
0.00
0.10
0.20
0.30
0.40
Fe3+ p.f.u.
Field of spinel from ES depleted xenoliths
reactions related to the host
LEGEND:
spinel from depleted xenoliths
spinel from pocket assemblages
spinel\oxide formed in reaction with the host
oxide from the host
3.0
2.5
2.0
1.5
1.0
0.5
0.0
0.00
0.05
0.10
0.15

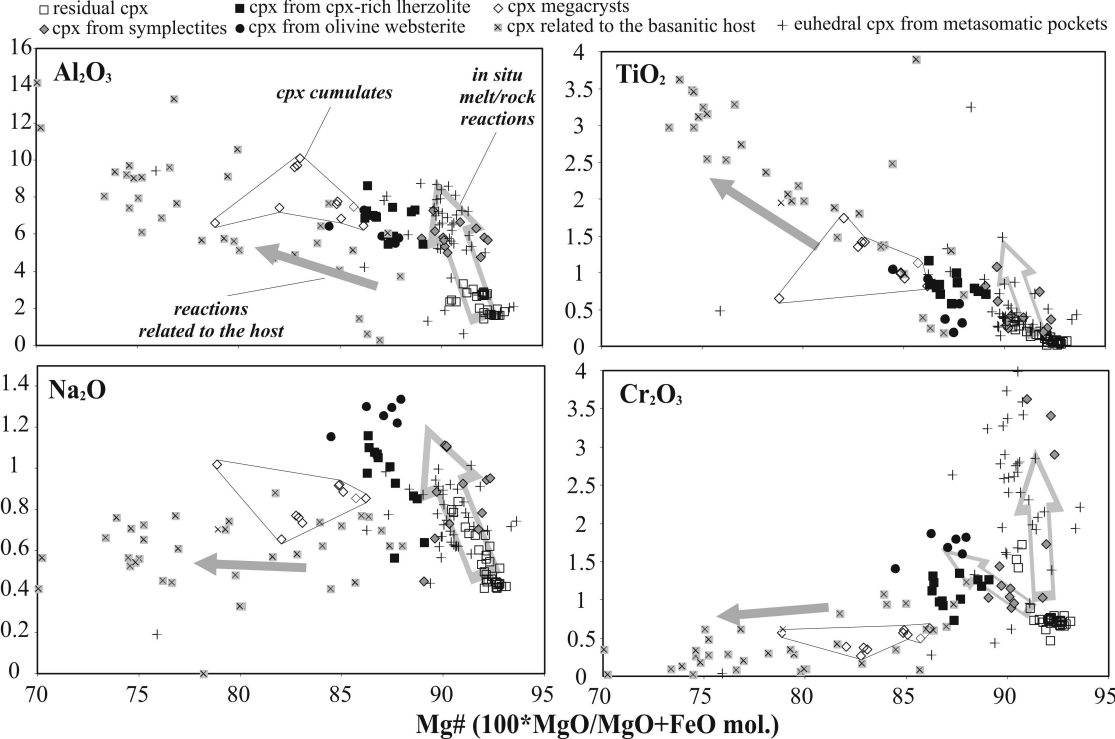
□ residual cpx
■ cpx from cpx-rich lherzolite
◇ cpx megacrysts
◆ cpx from symplectites
● cpx from olivine websterite
⊠ cpx related to the basanitic host
+ euhedral cpx from metasomatic pockets
Al2O3
cpx cumulates
in situ melt/rock reactions
reactions related to the host
TiO2
Na2O
Cr2O3
Mg# (100*MgO/MgO+FeO mol.)

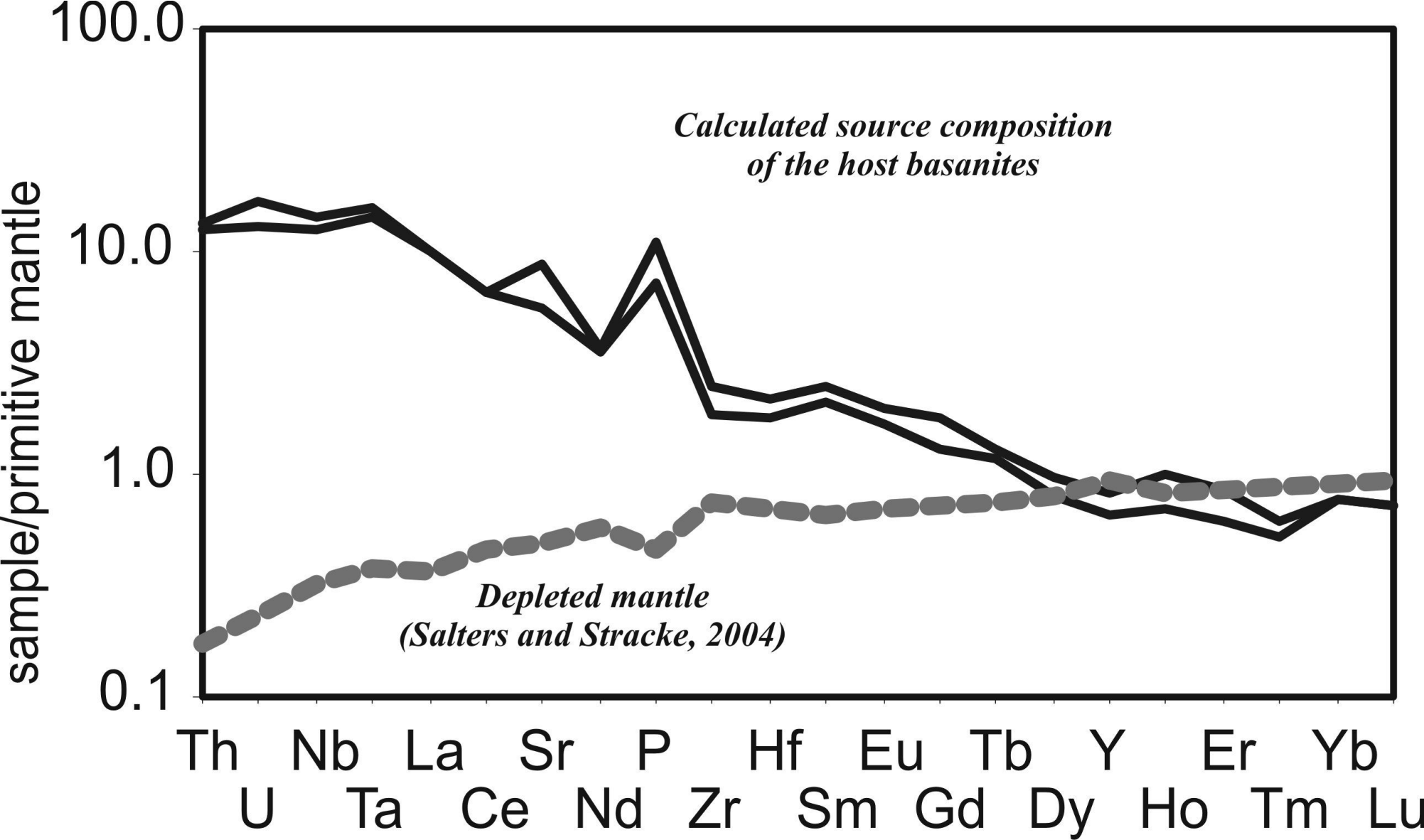
100.0
10.0
1.0
0.1
sample/primitive mantle
Calculated source composition
of the host basanites
Depleted mantle
(Salters and Stracke, 2004)
Th
U
Nb
Ta
La
Ce
Sr
Nd
P
Zr
Hf
Sm
Eu
Gd
Tb
Dy
Y
Ho
Er
Tm
Yb
Lu

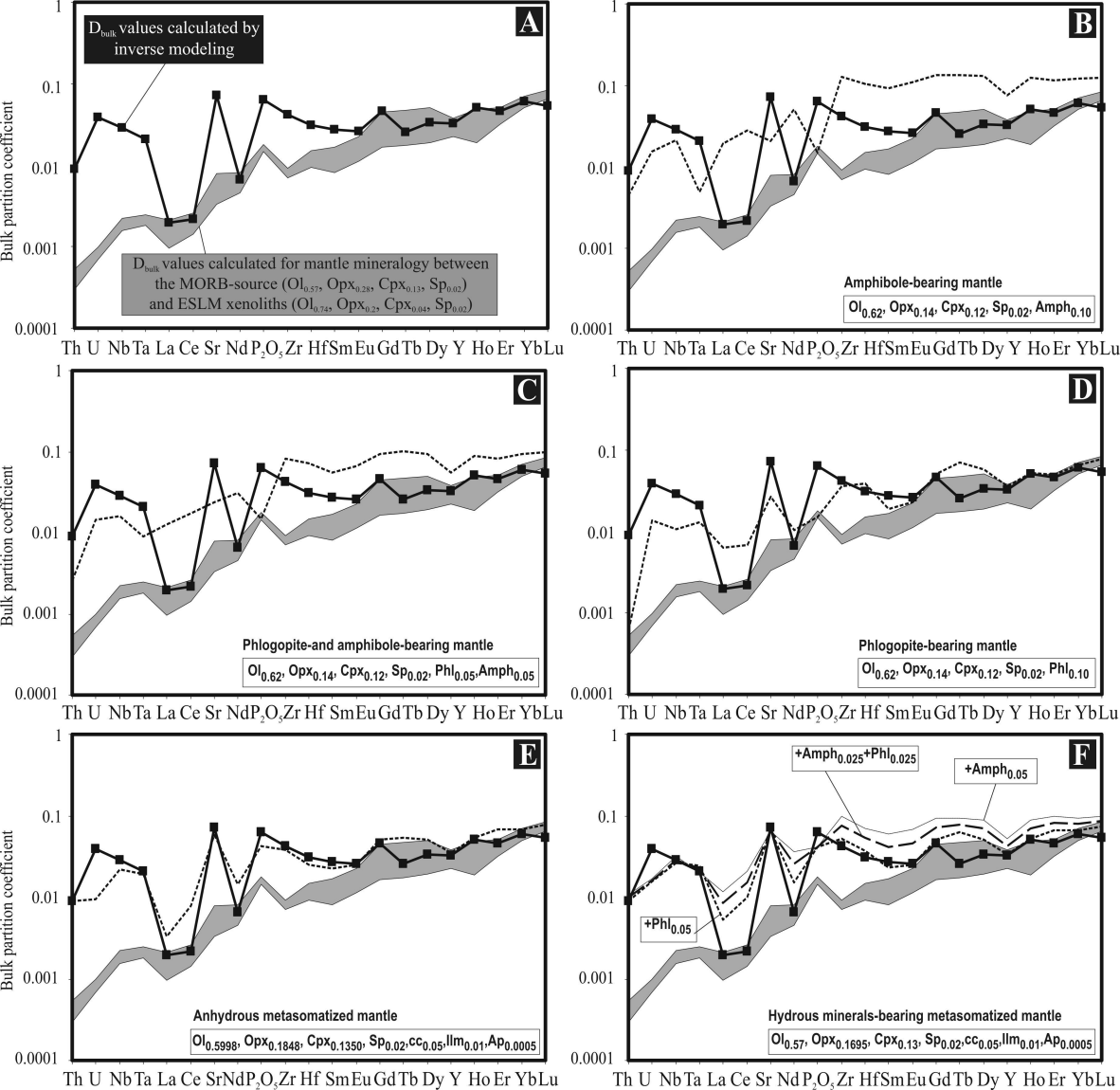
A
D_{bulk} values calculated by inverse modeling
D_{bulk} values calculated for mantle mineralogy between the MORB-source ($Ol_{0.57}$, $Opx_{0.28}$, $Cpx_{0.13}$, $Sp_{0.02}$) and ESLM xenoliths ($Ol_{0.74}$, $Opx_{0.2}$, $Cpx_{0.04}$, $Sp_{0.02}$)
B
Amphibole-bearing mantle
$Ol_{0.62}$, $Opx_{0.14}$, $Cpx_{0.12}$, $Sp_{0.02}$, $Amph_{0.10}$
C
Phlogopite-and amphibole-bearing mantle
$Ol_{0.62}$, $Opx_{0.14}$, $Cpx_{0.12}$, $Sp_{0.02}$, $Phl_{0.05}$,$Amph_{0.05}$
D
Phlogopite-bearing mantle
$Ol_{0.62}$, $Opx_{0.14}$, $Cpx_{0.12}$, $Sp_{0.02}$, $Phl_{0.10}$
E
Anhydrous metasomatized mantle
$Ol_{0.5998}$, $Opx_{0.1848}$, $Cpx_{0.1350}$, $Sp_{0.02}$,$cc_{0.05}$,$Ilm_{0.01}$,$Ap_{0.0005}$
F
$+Amph_{0.025}+Phl_{0.025}$
$+Amph_{0.05}$
$+Phl_{0.05}$
Hydrous minerals-bearing metasomatized mantle
$Ol_{0.57}$, $Opx_{0.1695}$, $Cpx_{0.13}$, $Sp_{0.02}$,$cc_{0.05}$,$Ilm_{0.01}$,$Ap_{0.0005}$
Bulk partition coefficient
1
0.1
0.01
0.001
0.0001
Th U Nb Ta La Ce Sr Nd P_2O_5 Zr Hf Sm Eu Gd Tb Dy Y Ho Er Yb Lu

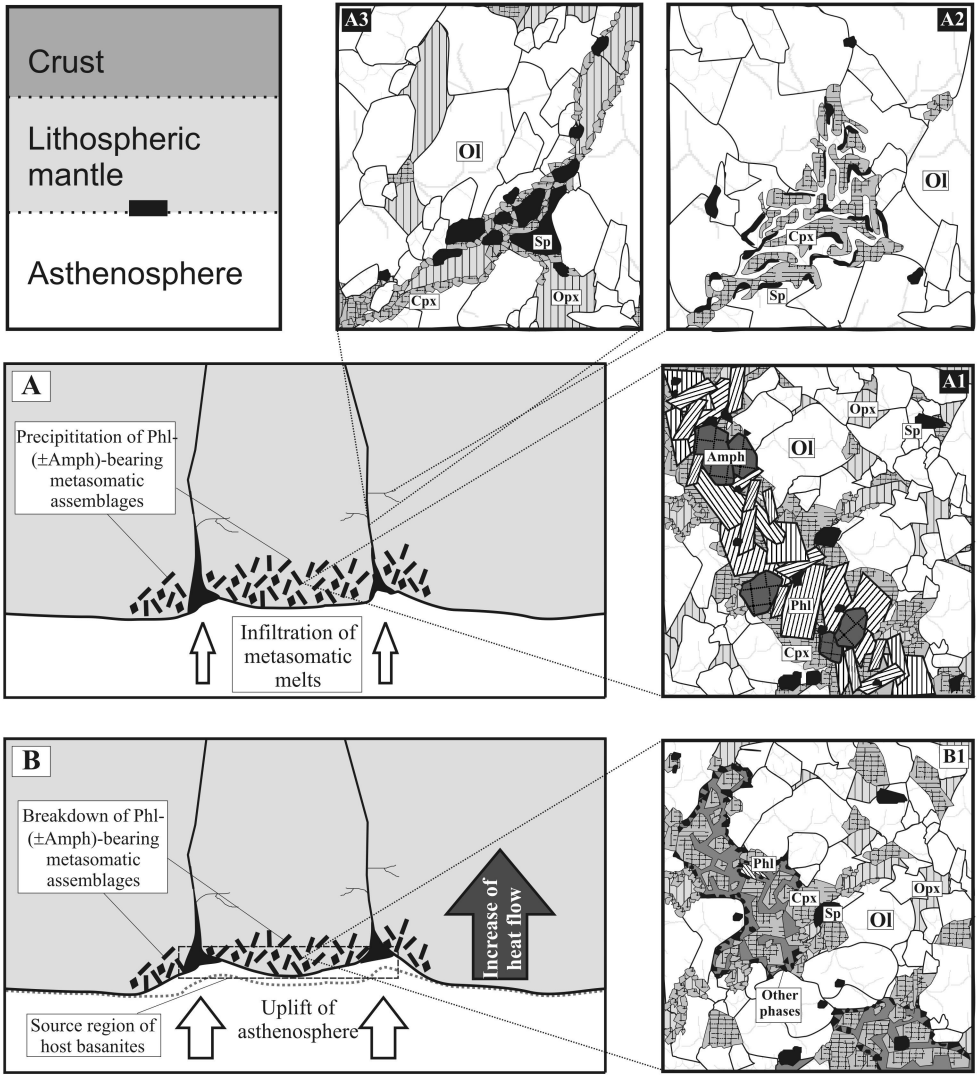
Crust
Lithospheric mantle
Asthenosphere
A3
Ol
Sp
Cpx
Opx
A2
Ol
Cpx
Sp
A
Precipititation of Phl-(±Amph)-bearing metasomatic assemblages
Infiltration of metasomatic melts
A1
Opx
Sp
Amph
Ol
Phl
Cpx
B
Breakdown of Phl-(±Amph)-bearing metasomatic assemblages
Increase of heat flow
Source region of host basanites
Uplift of asthenosphere
B1
Phl
Cpx
Sp
Opx
Ol
Other phases

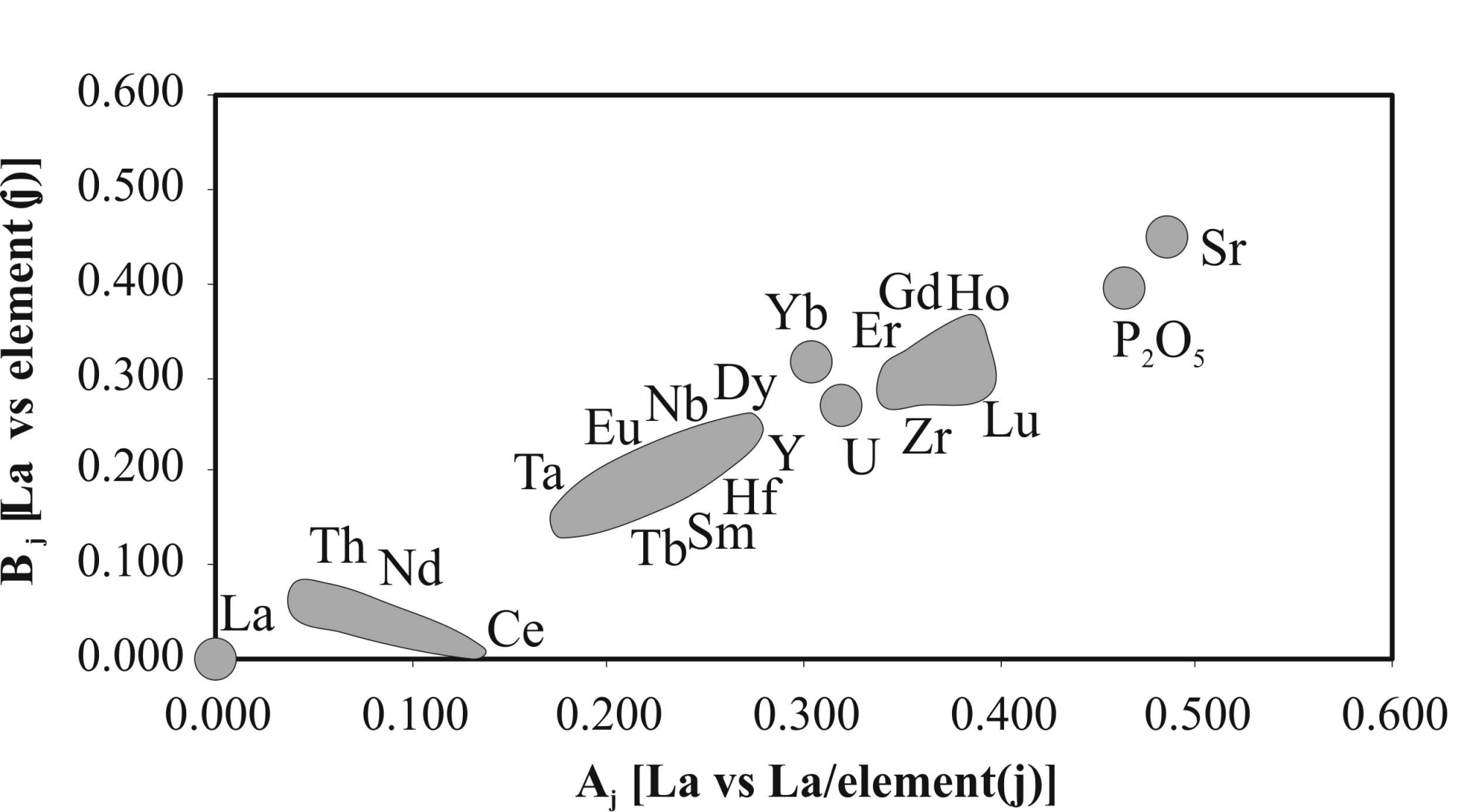
0.600
0.500
0.400
0.300
0.200
0.100
0.000
B_j [La vs element (j)]
0.000
0.100
0.200
0.300
0.400
0.500
0.600
A_j [La vs La/element(j)]
Sr
P_2O_5
Gd
Ho
Yb
Er
Dy
Nb
Eu
Ta
Y
U
Zr
Lu
Hf
Tb
Sm
Th
Nd
La
Ce

Table 1. *Main characteristics of xenoliths from East Serbian Paleogene basanites*

Xenolith type, equilibration T	Abundance, size, texture	Olivine	Orthopyroxene	Clinopyroxene	Spinel	Other minerals	Interpretation
Dunite/ Harzburgite/ Lherzolite, 950-1100 ^{o}C	Most abundant, ~90 % of the suite; few mm to 10 cm, protogranular, undeformed or slightly deformed	~75 vol% $Fo_{89.6-92}$	~20 vol% Mg#=90.5-92.5; Al_2O_3=1-2 wt%	<5 vol% Mg#=91-93 Al_2O_3 =1.4-3.4 wt%; Cr_2O_3 = 0.5-2 wt%	~1 vol% Cr#=0.5-0.7	Clinopyroxene, spinel, ±apatite, ± ilmenite, ±rutile, ±carbonate, ±glass (see text for detailed description)	More depleted mantle segment than most xenolith suites and peridotite massifs in Europe; Similar to modern sub-arc oceanic lithosphere.
Sp-poor, opx-rich olivine websterite, 800-1200 ^{o}C	Rare; 1-4 cm, protogranular to cumulitic, undeformed	<20 vol% Fo_{85-88}	~70-80 vol% Mg#=86-87; Al_2O_3=1.5-2.5 wt%	~5-10 vol% Mg#=85-92 Al_2O_3 =<1-4.4 wt%; Cr_2O_3 >1 wt%; TiO_2= 0.2-0.7 wt%	<<1 vol% Cr#=0.8-0.9; TiO_2= 0.3-11.5 wt%	Similar secondary minerals as in the first group, occurring in the interstices	Two-stage origin proposed: (I) lithospheric precipitation of a high-Mg, high-Si magma, and (II) subsequent metasomatism caused by CO_2- and alkali-rich melts
Sp-rich olivine websterite, 1050-1150 ^{o}C	Rare; 1-2 cm, protogranular, undeformed	<20 vol% Fo_{86-88}	~70-75 vol% Mg#~89; Al_2O_3=3-6 wt%	~10-20 vol% Mg#=87-88 Al_2O_3 ~ 5 wt%; Cr_2O_3 >1.5 wt%; TiO_2< 0.5 wt%	>2 vol% Cr#=0.3-0.35; TiO_2> 1 wt%	Similar secondary minerals as in the first group occurring in the interstices	Modification of the studied mantle by action of mafic alkaline melts; the high content of modal orthopyroxene is likely inherited .....
Cpx-rich lherzolite, 1000-1200 ^{o}C	Rare; 1-3 cm, protogranular, undeformed	~60 vol% Fo_{86-88}	~10-20 vol% Mg#=87-88; Al_2O_3> 4 wt%	~20- vol% Mg#=85-92 Al_2O_3 =5-7 wt%; Cr_2O_3 ≥1 wt%; TiO_2= ≥1 wt%	~2-3 vol% Cr#=0.15-0.2; TiO_2~ 0.5 wt%		Modification of the studied mantle by action of mafic alkaline melts.
Cpx (±olivine) megacrysts	Abundant, from <0.5 cm to >5 cm	Fo_{86}		Mg#=85-86 Al_2O_3 =6-10 wt%; Cr_2O_3 ~0.5 wt%; TiO_2= ~1 wt%			Deep seated cumulates from mafic alkaline magma.
Fe-rich dunite	Rare, 1-3 cm	>95 vol% Fo_{85-86}		<5 vol%; Composition similar to clinopyroxene megacrysts			Deep seated cumulates from mafic alkaline magma.

Table 2a. *Selected microprobe data of clinopyroxene occurring in various metasomatic associations in East Serbian xenoliths*

	Patchy metasomatic assemblages within depleted xenoliths									Clinopyroxene-spinel-olivine symplectites				
	SB-M-5					STZ-20-4		X-11/2		SB-M-3				
	1	2	3	4	5	6	7	8	9	10	11	12	13	14
SiO_2	49.72	49.30	50.55	47.44	48.37	47.20	48.29	47.51	48.82	52.19	51.82	50.18	50.84	50.76
TiO_2	0.40	0.28	0.85	1.33	0.28	0.44	0.35	0.42	1.48	0.25	0.29	0.81	0.61	0.74
Al_2O_3	6.61	7.12	5.20	7.83	7.42	8.66	8.08	8.57	6.49	5.32	5.80	5.75	6.18	6.28
FeO	2.98	2.95	3.05	3.52	3.02	2.74	2.57	2.56	2.92	3.08	3.06	3.24	3.14	2.48
MnO	0.07	0.03	0.08	0.09	0.08	0.06	0.03	0.07	0.05	0.11	0.12	0.06	0.09	0.05
MgO	15.46	15.12	15.77	13.78	15.06	13.78	14.25	13.80	14.84	16.43	16.23	15.09	15.77	15.79
CaO	20.60	21.07	21.12	20.02	21.14	21.14	21.31	21.01	22.47	20.20	20.00	23.32	21.12	21.81
Na_2O	0.73	0.82	0.87	0.98	0.94	1.00	0.90	0.92	0.57	1.10	1.11	0.45	0.89	0.70
Cr_2O_3	2.41	2.60	1.60	4.10	2.78	4.14	3.59	4.36	1.62	0.89	1.05	1.03	1.18	1.03
Total	99.04	99.39	99.19	99.17	99.15	99.21	99.46	99.27	99.28	99.65	99.54	99.97	99.87	99.71
Mg#	0.90	0.90	0.90	0.87	0.90	0.90	0.91	0.91	0.90	0.90	0.90	0.89	0.90	0.92

Table 2b. *Selected microprobe data of spinel occurring in various metasomatic associations in East Serbian xenoliths*

	Patchy metasomatic assemblages within depleted xenoliths							Clinopyroxene-spinel-olivine symplectites				Spinel-rich olivine websterite		
	X-6	X-11/2				K-19		SB-M-3				SB-3		
No	1	2	3	4	5	6	7	8	9	10	11	12	13	14
SiO_2	0.40	0.72	0.12	0.57	0.38	0.34	0.25	0.08	0.09	0.45	0.11	0.10	0.18	0.04
TiO_2	1.78	2.59	0.49	2.83	0.10	0.29	0.22	0.13	0.27	0.20	0.28	1.32	2.11	8.02
Al_2O_3	26.10	19.07	37.10	30.87	25.36	36.52	37.60	49.29	50.82	51.33	43.59	30.69	24.61	16.70
FeO^t	18.47	23.48	18.38	22.22	15.23	11.94	11.61	12.28	13.07	13.41	13.53	27.81	36.67	49.52
MnO	0.22	0.25	0.23	0.24	n.a.	n.a.	n.a.	0.12	0.17	0.16	0.13	0.39	0.52	0.60
MgO	14.19	12.47	16.21	13.40	14.82	17.53	17.84	20.73	19.74	20.32	19.44	12.47	9.59	7.23
Cr_2O_3	36.91	41.19	26.85	29.89	44.44	33.84	30.67	17.52	15.90	13.98	23.17	26.43	24.85	15.33
Total	98.09	99.78	99.39	100.02	100.33	100.46	98.18	100.14	100.06	99.84	100.25	99.21	98.53	97.44
Mg#	0.64	0.58	0.72	0.58	0.67	0.74	0.77	0.84	0.80	0.83	0.81	0.59	0.49	0.35
Cr#	0.49	0.59	0.33	0.39	0.54	0.38	0.35	0.19	0.17	0.15	0.26	0.37	0.40	0.38

Table 2c. *Selected microprobe data of carbonate and apatite occurring in patchy metasomatic assemblages within East Serbian xenoliths*

	Carbonate									Apatite				
	STZ-20-1				SB-M-5		K-19	X-20/10		STZ-20-1				
	1	2	3	4	5	6	7	8		1	2	3	4	5
SiO_2	0.04	0.17	0.05	0.04	0.00	0.02	0.05	0.02	**SiO_2**	0.45	0.93	1.70	0.44	0.92
Al_2O_3	0.02	0.02	0.02	0.05	0.00	0.01	0.02	0.01	**Al_2O_3**	0.02	0.07	0.36	0.01	0.08
FeO	0.11	0.07	0.14	0.51	0.12	0.08	0.31	0.11	**FeO**	0.31	0.28	0.58	0.24	0.17
MgO	1.42	1.20	1.32	13.14	2.34	1.42	1.38	2.08	**MgO**	0.19	0.31	0.97	0.20	0.23
CaO	57.10	58.30	57.85	44.72	56.73	57.65	55.59	55.26	**CaO**	54.38	53.67	53.10	54.96	54.93
P_2O_5	0.01	0.02	0.04	0.01	0.03	0.03	0.12	0.06	**P_2O_5**	39.55	40.60	35.64	40.31	40.00
Total	58.71	59.83	59.48	58.49	59.27	59.26	57.63	57.90	**Total**	94.95	95.92	92.40	96.19	96.44

Table 2d. *Selected microprobe data of feldspar, glass and ilmenite occurring in patchy metasomatic assemblages within East Serbian xenoliths*

	Feldspars				Glass					Ilmenite			
	K-19	X-11/2	X-20/10	X-20/11	K-19	X-11/2		X-20/5		STZ-20-1			
	1	2	3	4	5	6	7	8	9		1	2	3	4
SiO_2	56.98	65.69	65.14	53.80	61.57	52.82	61.61	59.24	53.27	**SiO_2**	0.06	0.05	0.07	0.44
TiO_2	0.08	0.10	0.65	0.10	0.25	1.38	2.28	0.24	0.10	**TiO_2**	55.16	55.45	53.24	50.68
Al_2O_3	27.07	20.38	19.80	28.45	16.77	18.32	21.45	24.83	28.15	**Al_2O_3**	0.04	0.05	0.06	0.16
FeO	0.37	0.20	0.15	0.41	0.38	1.58	0.22	0.31	0.41	**FeO**	35.67	34.90	37.37	38.12
MnO	0.02	0.00	0.02	0.03	0.03	0.08	0.11	0.03	0.02	**MnO**	0.66	0.64	0.90	0.90
MgO	0.06	0.02	0.01	10.79	3.36	11.31	0.00	5.96	10.63	**MgO**	8.36	8.71	7.67	6.09
CaO	8.67	0.58	0.67	10.79	4.74	0.65	0.93	5.96	10.63	**CaO**	0.38	0.96	0.04	0.10
Na_2O	5.72	5.62	5.65	4.72	4.47	1.64	2.73	6.30	3.95	**Na_2O**	b.d.l.	b.d.l.	b.d.l.	b.d.l.
K_2O	0.39	6.67	7.59	0.30	4.23	6.16	8.48	0.63	0.26	**K_2O**	b.d.l.	b.d.l.	b.d.l.	b.d.l.
Cr_2O_3	b.d.l.	b.d.l.	b.d.l.	b.d.l.	b.d.l.	b.d.l.	b.d.l.	b.d.l.	b.d.l.	**Cr_2O_3**	0.07	0.13	0.82	0.45
NiO	b.d.l.	b.d.l.	b.d.l.	b.d.l.	b.d.l.	b.d.l.	b.d.l.	b.d.l.	b.d.l.	**NiO**	0.14	0.16	0.07	0.09
Total	99.48	99.49	99.71	98.68	96.33	93.94	97.81	97.62	96.91	**Total**	100.57	101.09	100.28	97.26

Table 3a. *LA-ICP-MS trace element analyses of olivine from Fe-rich dunite (SB-M-1), clinopyroxene-spinel-olivine symplectite-bearing Mg-rich dunite (SB-M-3) and an average analysis of olivine from depleted harzburgite xenoliths (HZ: SB-M-4, SB-M-5); the forsterite contents are given in brackets*

	SB-M-1 (~Fo_{88})					SB-M-3 (~Fo_{91})					HZ (~$Fo_{>91}$)
ppm	Ol-1	Ol-2	Ol-3	Ol-4	Ol-5	Ol-1	Ol-2	Ol-3	Ol-4	Ol-5	Avr Ol
Li	2.01	2.04	2.16	2.19	2.11	1.07	1.22	1.22	1.20	1.24	1.78
Ca	1592	1583	1593	1591	1599	1075	998	1014	969	1005	771
Sc	5.89	5.78	5.89	5.79	5.95	5.6	5.4	5.5	5.6	6.1	3.96
Ti	48.6	48.7	52.5	49.7	49.9	7	6.07	5.7	8.57	11.7	4.26
Cr	296	295	288	294	289	167	164	155	155	158	73
Mn	1458	1497	1504	1532	1511	1164	1211	1237	1249	1251	1038
Ni	2703	2683	2642	2662	2589	3556	3506	3466	3452	3425	3713

Table 3b. *LA-ICP-MS trace element analyses of clinopyroxenes; data for clinopyroxene from spinel-poor olivine websterite xenoliths are from Cvetković et al. (in press) and are referring to clinopyroxene produced by orthopyroxene replacement (Type 1) and euhedral metasomatic clinopyroxene (Type 2)*

	Discrete clinopyroxene				Cpx from sympl.		Cpx from pockets			Cpx from sp-poor olivine websterites	
	SB-M-3						SB-M-4	SB-M-5			
ppm	Cpx-1	Cpx-2	Cpx-3	Cpx-4	Cpx-6	Cpx-7	Cpx-4	Cpx-3	Cpx-5	Type1	Type 2
Li	37.1	33.8	21.6	38.6	11.8	15.5	39.7	12	28.7	11.4	5.9
B	n.a.	n.a.	n.a.	n.a.	13.1	10.9	5.1	n.a.	4.1	3.9	4
Sc	86	96	97	96	84	98	94	81	105	93	94
V	n.a.	n.a.	n.a.	n.a.	682	370	281	n.a.	225	283	387
Cr	4979	5119	4628	4899	145779	24617	n.a.	4292	3480	n.a.	9368
Mn	648	666	695	727	1413	1221	1964	1186	1337	1528	939
Co	n.a.	n.a.	n.a.	n.a.	139	87	75	n.a.	35	26.1	40
Ni	517	479	446	525	2342	2168	1770	1084	1613	580	822
Cu	n.a.	n.a.	n.a.	n.a.	16.9	58.5	206	n.a.	206	35	11
Zn	n.a.	n.a.	n.a.	n.a.	310	32	103	n.a.	115	26	29
Rb	0.08	b.d.l.	0.06	0.11	0.64	1.07	1.22	4.04	2.92	11	3.9
Sr	258	193	136	218	400	197	208	382	212	103	98
Y	7.3	6.7	7	6.6	8.8	8.7	10.7	30	25.1	11	9.4
Zr	10.51	9.21	8.09	9.51	17.25	12.47	39.18	226	79	28	6.78
Nb	0.05	b.d.l.	0.06	0.17	1.16	1.37	7.93	60.6	27.4	8.85	1.14
Cs	n.a.	n.a.	n.a.	n.a.	0.04	0.06	0.14	n.a.	0.16	0.07	0.05
Ba	0.77	0.11	0.07	1.75	2.84	1.96	11.04	341	79	40.7	19.5
La	1.49	1.00	0.63	1.17	1.63	1.43	8.95	36.7	25.1	6.35	1.24
Ce	2.57	1.80	1.33	2.18	3.99	4.47	20.8	81.6	35.8	15.3	3.4
Pr	0.37	0.27	0.21	0.27	0.47	0.58	2.82	10.09	4.84	1.87	0.47
Nd	1.29	1.28	1.01	1.12	2.01	2.30	12.8	26.0	14.55	7.97	1.79
Sm	0.57	0.56	0.44	0.39	0.71	0.48	3.04	8.45	4.02	1.67	0.94
Eu	0.17	0.14	0.11	0.19	0.32	0.34	0.94	2.29	1.56	0.59	0.26
Gd	0.64	0.71	0.70	0.69	0.64	1.10	2.52	6.37	2.91	1.86	1.02
Tb	0.19	0.14	0.14	0.16	0.22	0.24	0.33	1.04	0.48	0.27	0.19
Dy	1.24	1.11	0.95	1.03	1.30	1.63	2.19	5.67	4.40	1.97	1.65
Ho	0.32	0.28	0.33	0.23	0.35	0.35	0.48	1.12	0.64	0.43	0.35
Er	0.88	0.80	0.68	0.81	0.88	1.07	1.26	2.86	1.67	1.02	0.95
Tm	0.14	0.13	0.09	0.13	0.17	0.18	0.18	0.41	0.36	0.15	0.20
Yb	0.73	0.99	0.88	0.88	1.21	1.23	0.91	2.46	1.26	1.10	1.39
Lu	0.16	0.18	0.21	0.15	0.17	0.18	0.13	0.45	0.35	0.20	0.23
Hf	0.45	0.36	0.30	0.26	0.56	0.51	0.94	4.10	1.44	0.85	0.20
Ta	b.d.l.	b.d.l.	b.d.l.	b.d.l.	0.10	0.08	0.61	3.35	1.39	0.43	0.00
Pb	0.30	0.22	0.27	0.47	2.45	3.80	2.97	2.28	3.67	0.57	0.96
Th	0.09	0.08	0.08	0.12	0.21	0.16	1.04	10.15	4.47	0.68	0.17
U	0.00	0.00	0.00	0.01	0.11	0.08	0.83	0.49	0.74	0.14	0.15

Table 4. *Major and trace element analyses of the Sokobanja mafic alkaline rocks used for modeling*

	X-2	X-12	SB-61	SB-62	SB-63	SB-64	SB-65	SB-66	SB-67
	1	2	9	10	11	12	13	14	15
SiO2	42.37	42.49	42.49	42.7	42.57	42.24	43.04	41.87	42.7
TiO2	1.78	1.88	1.83	1.82	1.84	1.87	1.72	1.68	1.66
Al2O3	13.01	13.72	13.74	13.51	13.5	12.99	13.6	12.73	12.71
Fe2O3	10.08	10.46	10.11	10.25	10.18	10.12	10	10.08	10.16
MnO	0.16	0.17	0.17	0.17	0.17	0.18	0.16	0.16	0.17
MgO	12.55	10.99	11.4	11.14	12.03	11.83	11.11	13.22	13.45
CaO	11.28	11.39	11.47	11.43	10.98	11.42	11.74	11.12	10.77
Na2O	3.2	3.63	3.74	3.78	3.49	3.58	3.7	2.98	3.08
K2O	0.64	0.81	0.73	0.76	0.71	0.81	0.77	0.9	0.74
P2O5	0.76	0.83	0.79	0.81	0.79	0.71	0.76	0.74	0.76
Mg#	0.71	0.68	0.69	0.68	0.70	0.70	0.69	0.72	0.72
Cr	567.9	417.4	458.4	458.4	478.9	521.5	492.6	622.6	608.9
Ni	303.1	218.5	213.7	197.7	230.2	241.2	218.2	295.1	293.9
Sc	23	22	20	20	20	22	21	20	20
Ba	710.8	745.5	761	774	805.9	837	826.8	839.6	790.9
Co	46.5	43.8	45.2	44	48.5	49.7	47.5	49.1	49.6
Cs	1.1	1.4	1.4	1.3	1.1	1.1	1.1	0.7	1.1
Ga	14.8	16.7	16.5	17.5	16.8	16.1	17	16.8	16
Hf	3.8	4.4	4.4	4.3	4.6	4.2	4.3	3.9	4.1
Nb	73.2	81.3	74.8	78.5	75.1	69	75.9	67.2	68.5
Rb	7.5	10.4	7.1	7.2	6.5	7.3	8.4	21.4	11.7
Sr	889.6	949.2	972.9	973.3	957.4	899	971	929.9	892.4
Ta	4	4.5	4.7	4.9	4.7	4.3	4.5	4.4	4.1
Th	9.9	9.3	11.2	10.5	9.9	8.6	9.6	9.3	8.9
U	2.2	2.4	2.5	2.4	2.6	2.2	2.4	2.3	2.5
V	196	206	197	206	206	203	212	194	188
W	1.1	1.2	1.7	2.3	1.4	0.9	2.6	0.8	1
Zr	170.4	189.2	178.8	182.5	177	166	176.5	161.1	159.1
Y	27.2	28.4	27.6	27.9	27.1	24.3	28	25.1	24.7
La	56.2	59.8	62.4	62.8	63.2	54	62	55	57.3
Ce	101.8	111	109.7	108.8	111	93	108.6	96.8	99.9
Pr	10.51	11.09	11.89	12.17	12.06	10.9	11.94	10.73	11
Nd	43	46.7	44.9	44.1	43.9	37.4	44	39.5	38.9
Sm	7.9	8.5	8.1	8.1	8	7.1	7.8	7.1	7.2
Eu	2.31	2.45	2.48	2.41	2.48	2.18	2.51	2.23	2.26
Gd	5.98	6.43	6.47	6.46	6.4	5.91	6.72	6.03	6.03
Tb	0.87	0.98	1	0.98	1.05	0.93	0.95	0.88	0.93
Dy	4.32	5.11	5.2	4.92	5.07	4.46	5.21	4.69	4.87
Ho	0.87	0.96	0.97	0.94	0.95	0.89	0.96	0.88	0.88
Er	2.28	2.51	2.46	2.4	2.6	2.03	2.54	2.28	2.37
Tm	0.36	0.39	0.35	0.36	0.37	0.3	0.33	0.32	0.32
Yb	2.11	2.33	2.04	2.16	2.21	1.96	2.23	2.02	1.9
Lu	0.31	0.32	0.34	0.33	0.34	0.3	0.36	0.3	0.3
Mo	2.9	3.4	2.8	2.9	2.7	2.6	2.3	1.7	1.7
Cu	52.5	47.8	47.6	45	46.7	54	55.3	51.1	51.9
Pb	3.7	3.5	3.4	2.9	3.2	3.4	3	3.5	3.5
Zn	61	64	59	59	59	63	52	62	61

Table 5. *Results of inverse modeling of the source composition of the host basanites; the minimal (MIN), maximal (MAX) and average (AVR) estimates of the bulk partition coefficient of the phases in the source (Do) and of the phases entering the melt (PL), as well as of the concentrations in the source; xCH are enrichment factors with respect of the chondrite composition (McDonoug & Sun, 1995)*

	D_o^{MIN}	D_o^{MAX}	D_o^{AVR}	P_L^{MIN}	P_L^{MAX}	P_L^{AVR}	C_o^{MIN}	C_o^{MAX}	C_o^{AVR}	xCH
Th	0.0088	0.0093	0.0091	0.0711	0.0184	0.0448	1.01	1.07	1.04	35.82
U	0.0340	0.0440	0.0390	0.2730	0.0591	0.1660	0.26	0.34	0.30	40.60
Nb	0.0270	0.0310	0.0290	0.2077	0.0904	0.1490	8.26	9.48	8.87	36.95
Ta	0.0200	0.0220	0.0210	0.1229	0.0352	0.0791	0.53	0.58	0.55	40.70
La	0.0020	0.0020	0.0020	0.0035	0.0035	0.0035	6.40	6.40	6.40	27.00
Ce	0.0022	0.0022	0.0022	0.0040	0.0040	0.0040	11.08	11.08	11.08	18.08
Sr	0.0570	0.0880	0.0725	0.4156	0.0978	0.2567	112.69	173.98	143.34	19.77
Nd	0.0065	0.0067	0.0066	0.0418	0.0123	0.0271	4.43	4.57	4.50	9.85
P	0.0500	0.0770	0.0635	0.4060	0.0852	0.2456	0.08	0.13	0.11	0.00
Zr	0.0360	0.0480	0.0420	0.3021	0.0695	0.1858	19.53	26.04	22.78	5.96
Hf	0.0280	0.0340	0.0310	0.2069	0.0370	0.1220	0.51	0.62	0.56	5.45
Sm	0.0250	0.0300	0.0275	0.1953	0.0344	0.1148	0.85	1.01	0.93	6.29
Eu	0.0240	0.0280	0.0260	0.1936	0.0591	0.1263	0.26	0.30	0.28	4.96
Gd	0.0390	0.0540	0.0465	0.3207	0.0594	0.1900	0.70	0.97	0.83	4.19
Tb	0.0240	0.0270	0.0255	0.1486	0.0422	0.0954	0.11	0.13	0.12	3.38
Dy	0.0300	0.0370	0.0335	0.2408	0.0637	0.1523	0.53	0.65	0.59	2.41
Y	0.0290	0.0360	0.0325	0.2434	0.0608	0.1521	2.86	3.54	3.20	2.04
Ho	0.0420	0.0600	0.0510	0.3511	0.0730	0.2120	0.10	0.15	0.13	2.33
Er	0.0380	0.0530	0.0455	0.3214	0.0536	0.1875	0.27	0.38	0.32	2.02
Yb	0.0605	0.0605	0.0605	0.0640	0.0640	0.0640	0.34	0.34	0.34	2.08
Lu	0.0540	0.0540	0.0540	0.0600	0.0600	0.0600	0.05	0.05	0.05	1.96

Table 6. *Bulk mineral-melt partition coefficients used for calculation of source mineralogy for host basanites*

	Ol	Opx	Cpx	Sp	Amph	Phl	Ilm	cc	Ap
Th	0.00005	0.0009	0.002		0.04	0.0014	0.0006		19
U	0.00005	0.0032	0.0006		0.15	0.13	0.0082		16
Nb	0.0004	0.0033	0.0052	0.02	0.196	0.088	2		
Ta	0.0004	0.0049	0.0035	0.02	0.03	0.1096	1.7		
La	0.0001	0.001	0.0123	0.01	0.17	0.0413	0.000029		2.5
Ce	0.0003	0.0039	0.01	0.001	0.26	0.0455	0.000054		11.2
Sr	0.001	0.003	0.05		0.12	0.183	0	1	1.1
Nd	0.001	0.012	0.031	0.01	0.44	0.0293	0.0005		14
P	0.01	0.03	0.03				0.05		50
Zr	0.0033	0.0167	0.016	0.03	1.2	0.2806	3.002		0.986
Hf	0.001	0.033	0.035	0.03	0.92	0.2703	1.18		0.878
Sm	0.001	0.019	0.082	0.01	0.76	0.0255	0.0006		14.6
Eu	0.0015	0.03	0.1	0.01	0.88	0.0218	0.0011		9.6
Gd	0.0015	0.016	0.3	0.01	0.86	0.0205	0.0034		15.8
Tb	0.0015	0.019	0.31	0.01	0.83	0.2	0.0067		15.4
Dy	0.0017	0.022	0.33	0.01	0.78	0.0281	0.01		3.9
Y	0.0099	0.0455	0.15		0.396	0.007	0.0045		
Ho	0.0016	0.026	0.31	0.01	0.73		0.011		13.4
Er	0.0132	0.0717	0.182	0.01	0.68	0.0303	0.0275		41.6
Yb	0.0305	0.1013	0.18	0.01	0.59	0.0484	0.17		8.1
Lu	0.043	0.127	0.18	0.01	0.51	0.0471	0.084		3.8

Explanation and data sources: $D_{mineral/melt}$ for olivine (Ol), orthopyroxene (Opx), and clinopyroxene (Cpx) from Keshav *et al.* (2005) and references therein, except for Gd, Tb, Dy and Ho (McKenzie & O'Nions 1991) and for P (Ulmer 1989); $D_{mineral/melt}$ for spinel (Sp) are after McKenzie & O'Nions (1991) except for Nb, Ta, Zr and Hf (Horn *et al.* 1994); $D_{mineral/melt}$ for amphibole (Amph) from McKenzie & O'Nions (1991) except for Th (La Tourette *et al.* 1995), U, Zr and Hf (Villemant *et al.* 1981), Nb and Y (Chazot *et al.* 1996) and Ta (Green *et al.* 1993); $D_{mineral/melt}$ for phlogopite (Phl) from Fujimaki *et al.* (1984) except for Th and Nb (La Tourette *et al.* 1995), U and Tb (Villemant *et al.* 1981) and for Ta, Sr and Y (Foley *et al.* 1996); $D_{mineral/melt}$ for ilmenite (Ilm) from Zack & Brumm (1998) except for P (Anderson & Greenland 1969) and for Zr and Hf (Fujimaki *et al.* 1984); The values for $D_{mineral/melt}$ for calcite (cc) are considered too low for all elements except for Sr which is considered to be unity (e.g. Ionov & Harmer 2002); $D_{mineral/melt}$ for apatite (Ap) from Paster *et al.* (1974) except for Th, U (average values from Luhr *et al.* 1984; Bea *et al.* 1994; Mahood & Stimac 1990), Sr, Dy and Lu (Watson & Green 1981), Zr, Hf and Er (Fujimaki 1986) and for P for which $D_{mineral/melt}$ was calculated on the basis of P_2O_5 concentrations in apatite from ESLM xenoliths and in host basanites. Missing $D_{mineral/melt}$ values are considered not important for the calculations because of low element partition into given minerals.

Appendix/Table. *Results of inversion modeling of the source composition of the host basanites; the minimal (MIN), maximal*

	Aj	Bj	r		Aj	Bj
Th	0.156	0.485	0.701	La/Th	0.0067	5.732
U	0.029	0.699	0.757	La/U	0.1224	17.548
Nb	0.958	17.047	0.729	La/Nb	0.0031	0.62
Ta	0.063	0.727	0.780	La/Ta	0.0362	11.158
Ce	1.743	1.340	0.931	La/Ce	0.00002	0.56526
Sr	8.444	437.360	0.862	La/Sr	0.0005	0.0336
Nd	0.671	2.789	0.775	La/Nd	0.001	1.3334
P2O5	0.008	0.329	0.738	La/P2O5	0.5582	43.612
Zr	1.996	55.287	0.720	La/Zr	0.0018	0.233
Hf	0.054	1.027	0.769	La/Hf	0.0557	10.73
Sm	0.102	1.720	0.730	La/Sm	0.0273	6.025
Eu	0.032	0.479	0.930	La/Eu	0.0861	19.896
TiO2	0.006	1.438	0.261	La/TiO2	0.4403	7.1075
Gd	0.071	2.083	0.898	La/Gd	0.0539	6.2438
Tb	0.013	0.182	0.820	La/Tb	0.2045	50.087
Dy	0.062	1.256	0.871	La/Dy	0.0523	8.9451
Y	0.334	6.934	0.773	La/Y	0.0094	1.6603
Ho	0.010	0.335	0.872	La/Ho	0.3972	40.649
Er	0.028	0.780	0.842	La/Er	0.1376	16.355
Tm	0.005	0.064	0.596	La/Tm	0.4837	143.8
Yb	0.023	0.761	0.591	La/Yb	0.1736	17.87
Lu	0.004	0.101	0.754	La/Lu	1.0765	123.93